

Response to the Editor's Comments

1. Editor's comment: Motivate (briefly) why EW is suitable for your reconstruction, e.g. by informing when the EW is formed..

Author's Response: Thank you very much for the suggestion. We added the formation period of EWW in the *Introduction* section. Please refer to Line10 on Page 3.

2. Editor's comment: The reconstruction is "biased" towards wet values, especially in its early part (see e.g. table 4). This is not well reflected in the other hydroclimate reconstructions you compare with, and the EWW data does not seem to fully capture the observed dry years. Is this real or due to the data? It could be good to briefly discuss this point.

Author's Response: Thank you for the question. One possible reason is that the reconstruction has underestimated the drought severity in its early part. This may be due to the low-frequency hydroclimatic signals being removed during the detrending process when using simple curve fitting methods (Briffa et al., 1996). The Regional Curve Standardization (RCS) method might preserve more low-frequency signals (Briffa et al., 1992), but it requires more field work. We added the relevant discussion in Line 7-13 on Page 11.

3. Editor's comment: To make the paper more accessible, you should consider letting a native speaker go through the text. It is generally very well written, but still there is room for improvement.

Author's Response: Thank you for suggestion. We asked a professional English editing company to improve the English writing completely. The *editorial certificate* is attached as follows.



EDITORIAL CERTIFICATE

This document certifies that the manuscript listed below was edited for proper English language, grammar, punctuation, spelling, and overall style by one or more of the highly qualified native English speaking editors at EditSprings.

Manuscript title:
Early summer hydroclimatic signals were well captured by tree-ring earlywood width in the eastern Qinling Mountains, central China

Authors:
Yesi Zhao, Jiangfeng Shi, Shiyuan Shi, Xiaoqi Ma, Weiye Zhang, Bowen Wang, Xuguang Sun, Huayu Lu, Achim Bräuning

Date Issued:
May 29 2019

Certificate Number:
ES-201905231612688554



This certificate can be verified on www.editsprings.com/query.asp. This document certifies that the manuscript listed above was edited for proper English language, grammar, punctuation, spelling, and overall style by one or more of the highly qualified native English speaking editors at EditSprings. Neither the research content nor the authors' intentions were altered in any way during the editing process. Documents receiving this certification should be English-ready for publication; however, the author has the ability to accept or reject our suggestions and changes.

EditSprings provides a range of editing, translation and manuscript services for researchers and publishers around the world. Our top-quality PhD editors are all native English speakers from famous institutions across the U.S., Britain, Canada and so on. Our editors come from nearly every research field and possess the highest qualifications to edit research manuscripts written by non-native English speakers.

4. Editor's comment: Note that the figures should be able to stand on their own, so all necessary information (including relevant references) need to be in the figure captions.

Author's Response: Thank you for the suggestion. We rechecked all the figure captions again. A complete caption description was added for Fig.4.

5. Editor's comment: In the first section you refer to Liu et al. 2018b before 2018a, please change and have a general look at the references throughout.

Author's Response: Thank you for the suggestion. We sorted the reference using the LaTeX package provided by the journal CP. "*Liu, X et al. 2018 (Liu et al., 2018a)*" was automatically put before "*Liu, Y et al., 2018 (Liu et al., 2018b)*" in the reference list. Since we cited "*Liu, Y et al., 2018 (Liu et al., 2018b)*" firstly and "*Liu, X et al. 2018 (Liu et al., 2018a)*" secondly in the text, "*Liu et al., 2018b*" naturally came in front of "*Liu et al., 2018a*".

6. Editor's comment: I strongly recommend that you make the data presented in this paper available through an open repository rather than "on request", at least the data plotted in Fig. 6c.

Author's Response: Thank you for the suggestion. We added the MJJ scPDSI reconstruction in the supplementary materials.

Note: The regional annual mean precipitation (Line 20, Page 3) and the Figs. 2, 3 and 4 were updated because we corrected the average of precipitation data. According to Jones and Hulme (1996), regional precipitation series can be calculated by firstly deriving the regional averages in terms of percentages, then multiplying the regional mean to transform the resulting series back to millimeter units. In the previous versions, however, we misused "standard deviation" rather than "mean" as the denominator to calculate percentages. The correction has an influence on the regional annual and monthly mean precipitation amount, but a very slight impact on precipitation variation and its correlation with tree-ring width series. The correction does not change the results and conclusions.

Thank you again for your careful review and valuable suggestions for the manuscript.

Reference :

Briffa, K. R., Jones, P. D., Bartholin, T. S., Eckstein, D., Schweingruber, F. H., Karlén, W., Zetterberg, P., and Eronen, M.: Fennoscandian summers from AD 500: temperature changes on short and long timescales, *Clim. Dynam.*, 7, 111–119, <https://doi.org/10.1007/BF00211153>, 1992.

Briffa, K. R., Jones, P. D., Schweingruber, F. H., Karlén, W., and Shiyatov, S. G.: Tree-ring variables as proxy-climate indicators: problems with low-frequency signals, in: *Climatic variations and forcing mechanisms of the last 2000 years*, edited by: Jones, P. D., Bradley, R. S., and Jouzel, J., Springer, Berlin, Heidelberg, 9–41, http://doi.org/10.1007/978-3-642-61113-1_2, 1996.

Jones, P. D., and Hulme, M.: Calculating regional climatic time series for temperature and precipitation: methods and illustrations, *Int. J. Climatol.*, 16, 361–377, [https://doi.org/10.1002/\(SICI\)1097-0088\(199604\)16:4<361::AID-JOC53>3.0.CO;2-F](https://doi.org/10.1002/(SICI)1097-0088(199604)16:4<361::AID-JOC53>3.0.CO;2-F), 1996.

Early summer hydroclimatic signals are well captured by tree-ring earlywood width in the eastern Qinling Mountains, central China

Yesi Zhao^{1,2}, Jiangfeng Shi^{1,3}, Shiyuan Shi¹, Xiaoqi Ma¹, Weijie Zhang¹, Bowen Wang¹, Xuguang Sun⁴, Huayu Lu¹, Achim Bräuning²

- 1 School of Geography and Ocean Science, Nanjing University, Nanjing 210023, China
- 2 Institute of Geography, Friedrich-Alexander-University Erlangen-Nürnberg, Erlangen 91058, Germany
- 3 Laboratory of Tree-Ring Research, University of Arizona, Tucson 85721, USA
- 4 School of Atmospheric Sciences, Nanjing University, Nanjing 210023, China

Correspondence to: Jiangfeng Shi (shijf@nju.edu.cn)

10 **Abstract.** In the humid and semi-humid regions of China, tree-ring width (TRW) chronologies offer limited moisture-related climatic information. To gather additional climatic information, it would be interesting to explore the potentials of the intra-annular tree-ring width indices (i.e., the earlywood width (EWW) and latewood width (LWW)). To achieve this purpose, TRW, EWW and LWW were measured from the tree-ring samples of *Pinus tabulaeformis* originating from the semi-humid eastern Qinling Mountains, central China. Standard (STD) and signal-free (SSF) chronologies of all parameters were created using

15 these detrending methods including (1) negative exponential functions combined with linear regression with negative (or zero) slope (NELR), (2) cubic smoothing splines with a 50 % frequency cutoff at 67 % of the series length (SP67), and (3) age-dependent splines with an initial stiffness of 50 years (SPA50). The results showed that EWW chronologies were significantly negatively correlated with temperature, but positively correlated with precipitation and soil moisture conditions during the current early growing season. By contrast, LWW and TRW chronologies had weaker relationships with these climatic factors.

20 The strongest climatic signal was detected for the EWW STD chronology detrended with the NELR method, explaining 50 % of the variance of the May–July self-calibrated Palmer Drought Severity Index (MJJ scPDSI) during the instrumental period 1953–2005. Based on this relationship, the MJJ scPDSI was reconstructed back to 1868 using a linear regression function. The reconstruction was validated by comparison with other hydroclimatic reconstructions and historical document records from adjacent regions. Our results highlighted the potentials of intra-annual tree-ring indices for reconstructing seasonal hydroclimatic variations in humid and semi-humid regions of China. Furthermore, our reconstruction exhibited a strong in-phase relationship with a newly proposed East Asian summer monsoon index (EASMI) before the 1940s on the decadal and longer timescales, which may be due to the positive response of the local precipitation to EASMI. Nonetheless, the cause for the weakened relationship after the 1940s is complex, and cannot be solely attributed to the changing impacts of precipitation and temperature.

25

30

删除了: were

删除了: T

删除了: could only provide

删除了: amount of

删除了: in the humid and semi-humid regions of China;

删除了: thus,

删除了: is

删除了: worth

删除了: to

删除了: provide some additional climatic information. To fulfil this task,

删除了: in a semi-humid region

删除了: , that is, the

删除了: Their s

删除了: created

删除了: different

删除了: together

删除了: smoothed

删除了: of

删除了: Comparatively

删除了: with

删除了: detrending method of

删除了: contained the strongest climatic signal

删除了: t

删除了: further

删除了: ng

删除了: in

删除了: This

删除了: reconstruction

删除了: the

删除了: However

删除了: complicated

1 Introduction

Most of the existing tree-ring width (TRW) based hydroclimatic reconstructions ~~in China were~~ conducted ~~for~~ the regions ~~located between~~ the 200-to 600-mm annual precipitation isolines (Liu et al., 2018b), close to the northern fringe of Asian Summer Monsoon ~~realm~~. ~~Nonetheless~~, there ~~exists still a small number of~~ hydroclimate reconstructions in the core monsoon region, for example ~~from~~ Southeast China (e.g., Cai et al., 2017; Chen et al., 2016a; Shi et al., 2015), North China (e.g., Chen et al., 2016b; Hughes et al., 1994; Lei et al., 2014; Liu et al., 2002), and ~~from~~ the Hengduan mountains in Southwest China (e.g., Fan et al., 2008; Fang et al., 2010b; Gou et al., 2013; Li et al., 2017). Since precipitation is spatially ~~highly~~ variable (Ding et al., 2013), hydroclimatic variations ~~close to the~~ monsoon ~~boundary~~, cannot completely represent those in the core monsoon region (Liu et al., 2018b). Thus, ~~additional~~ hydroclimatic reconstructions are needed ~~from the center of~~ the monsoon region.

Some TRW chronologies within the monsoon region showed weak or unstable hydroclimatic signals (e.g., Li et al., 2016; Shi et al., 2012; Wang et al., 2018), ~~making them~~ unsuitable ~~to derive~~ reliable reconstructions. ~~By contrast~~, ~~intra-annually~~ resolved tree-ring width (i.e., earlywood width (EWW) and latewood width (LWW)), ~~provided~~ stronger hydroclimatic signals than TRW in some cases (Chen et al., 2012; Zhao et al., 2017a). This might be ~~because the~~ movement of ~~the~~ monsoon rain belt ~~can lead~~ ~~to an uneven distribution of precipitation during the growing season~~ (Jiang et al., 2006), ~~thus causing restrictions of water availability during parts of the growing season, and limiting the growth of certain intra-ring sectors rather than of total ring width~~ (Liu et al., 2018a). EWW and LWW ~~have been~~ successfully applied for reconstructing long-term variations of seasonal rainfall (Hansen et al., 2017), ~~drought~~ (standardized precipitation evapotranspiration index SPEI; Zhao et al., 2017b), and streamflow (Guan et al., 2018) ~~in~~ the monsoon region.

The eastern Qinling Mountains are located within the core region of ~~the~~ East Asian summer monsoon (EASM), and are characterized by a transitional climate from warm-temperate to subtropical. In this region, Shi et al. (2012) ~~built~~ four TRW chronologies of *Pinus tabulaeformis* along an elevation gradient from 1200 to 1950 m above sea level (a.s.l.). The TRW chronologies ~~of~~ the two low-altitude sites, ~~i.e.~~, Baiyunshan and Longchiman, exhibited a positive response to precipitation and negative response to temperature during early summer, showing ~~the sign of~~ water stress. However, the dendroclimatic potentials of EWW and LWW were not explored.

~~Meanwhile~~, tree-growth at an adjacent site was found to be more restricted by the drought index, ~~represented by the well-known~~ PDSI (Palmer Drought Severity Index), ~~rather than~~ ~~by~~ precipitation ~~or~~ temperature (Peng et al., 2014). ~~Briefly~~, ~~the~~ PDSI monitors the cumulative departure of surface water balance in terms of the difference between the amount of precipitation required to retain a normal water-balance level and the amount of actual precipitation (Palmer, 1965; Wells et al., 2004). In addition, the SPEI, ~~a drought index representing~~ water balance ~~in~~ the form of difference between precipitation and potential evapotranspiration (Vicente-Serrano et al., 2010), ~~was reported to constrain~~ latewood growth at a well-drained site in the core region of EASM (Zhao et al., 2017a, b). ~~According to these findings, complex drought indices like~~ the PDSI and SPEI should also be incorporated into the climate-tree-growth relationship assessment ~~of tree-ring variables~~.

删除了: have been

删除了: in

删除了: , a few case studies in

删除了: in the

删除了: fringe

删除了:

删除了: more

删除了: in

删除了: to be used for

删除了: I

删除了: , however,

删除了: related to

删除了: seasonal

删除了: which

删除了: causes restrictions of water availability through the growing season (Liu et al., 2018a)

删除了: Using

删除了: , researchers have successfully conducted reconstructions for ...

删除了: standardized precipitation evapotranspiration index

删除了: within

删除了: has

删除了: from

删除了: some kind of

删除了: Meanwhile, t

删除了: and

删除了: T

删除了: which represents

删除了: as

删除了: has

删除了: also been found to strongly limit

删除了: Therefore,

Recently, a new East Asian summer monsoon index (EASMI) based on the 200 hPa zonal wind anomalies was introduced by Zhao et al. (2015). The new EASMI performs better in describing precipitation and temperature variations over East Asia than existing indices. Suppose a strong EASM occurred, the new EASMI would indicate abundant precipitation and relatively low temperature over the core region of EASM, particularly around the area of mei-yu/changma/baiu rainband (27.5°–32.5° N, 105°–120° E and 30°–37.5° N, 127.5°–150° E; Fig. 1a), which is the center of the leading mode of EASM precipitation (Wang et al., 2008; Zhao et al., 2015). It would be interesting to study the response of local hydroclimate to EASM from a long-term perspective in combination with these tree-ring materials and the new EASMI. Considering the TRW series of *P. tabulaeformis* in Baiyunshan and Longchiman are mainly restricted by the early summer moisture conditions, we hypothesize that the early summer hydroclimatic signals might be strengthened only using EWW, since earlywood is mostly formed before mid-July (Zhang et al., 1982). Therefore, the objectives of this study are (1) to verify that EWW is more sensitive to early summer hydroclimatic factors than TRW and LWW for *P. tabulaeformis* at Baiyunshan and Longchiman, (2) to reconstruct early summer hydroclimate variations using EWW, and (3) to tentatively explore the relationship between the reconstructed hydroclimate variability and EASMI.

2 Materials and Methods

2.1 Study sites

In this study, the dated tree-ring samples of *P. tabulaeformis* are those presented by Shi et al. (2012). Briefly, they were collected from two sampling sites in Mount Funiu in 2006 and 2008 separately: Baiyunshan (33.63° N, 111.85° E) and Longchiman (33.68° N, 112.05° E; Fig. 1b). The sampling sites are located on mountain tops, where soils are thin and well-drained. The elevations of Baiyunshan and Longchiman range 1200–1300 m a.s.l., and 1340–1400 m a.s.l., respectively. The regional annual mean temperature and annual total precipitation are 14.1 °C and 809.1 mm, respectively. Most of the annual total precipitation drops in the warm season (Fig. 2). More detailed information of the study sites can be found in Shi et al. (2012).

2.2 Tree-ring data

P. tabulaeformis is a widely distributed conifer species in North China with the extension from 31° 00' N to 43° 33' N, and 103° 20' E to 124° 45' E (Xu et al., 1981). By studying the cambial dynamics of *P. tabulaeformis* in its northern distribution limit (43° 14.11' N, 116° 23.60' E, 1363 m a.s.l.), Liang et al. (2009) reported that the cell division in the cambial zone would start within the third week of May and complete by mid-September. A separate study in Northwest China (37° 02' N, 104° 28' E, 2456 m a.s.l.) found that the cambial cells of mature *P. tabulaeformis* would start the cell division in late spring and cease in late July/early August (Zeng et al., 2018). Since our sampling sites are located at lower latitudes, the cambial activity of *P. tabulaeformis* in our study area may start earlier and end later than those found in above studies (following the temperature-controlled phenology theory; Chen and Xu, 2012).

删除了: performance

删除了: When

删除了: s

删除了: is worth

删除了: Since

删除了: of Zhao et al. (2015)

删除了: Dated

删除了: used in this study were previously

删除了: in

删除了: T

删除了: from

删除了: 22

删除了: The majority part of the

删除了: during

删除了: The selected

删除了: Liang et al. (2009) studied

删除了: and found

删除了: ed

删除了: did not

删除了: around

删除了: Zeng et al. (2018)

删除了: in Northwest China (37° 02' N, 104° 28' E, 2456 m a.s.l.)

删除了: ed

删除了: activity

删除了: d

删除了: to

删除了: Considering that

删除了: es

删除了: s

删除了: according

删除了: to

删除了: (

P. tabulaeformis generally exhibits an abrupt transition from light-colored earlywood to dark-colored latewood (Fig. S1; Liang and Eckstein, 2006). Based on the characteristics of the tree-ring anatomy, the earlywood and latewood segments of annual growth rings can be distinguished visually by the sudden change in cell size, lumen size, and color (Stahle et al., 2009). However, gradual transitions could occur in a few samples, making the earlywood-latewood boundary difficult to differentiate.

Therefore, only samples with distinct earlywood and latewood segments were used for subsequent measurements (Knapp et al., 2016). In total, 20 cores from 11 trees and 42 cores from 22 trees were selected from Baiyunshan and Longchiman, respectively. EWW and LWW were then measured using a LINTAB5 system at a resolution of 0.001 mm, and TRW was obtained by adding EWW and LWW of the same calendar years together.

2.3 Development of tree-ring width chronologies

Non-climatic growth trends need to be fitted and removed from each “raw” (untreated) EWW, LWW and TRW series, which is known as detrending (Cook et al., 1990). To check the effects of detrending methods on the preservation of climatic signals, three detrending methods were selected for comparison. These included were negative exponential functions combined with linear regression with negative (or zero) slope (NELR), cubic smoothing splines with a 50 % frequency cutoff of 67 % of the series length (SP67), and age-dependent splines with an initial stiffness of 50 years (SPA50). NELR is a deterministic method based on the assumption that tree radial growth declines monotonically (Cook et al., 1990). SP67 has a good ability in fitting the potential low-and middle-frequency perturbations contained in ring-width series (Cook et al., 1990). It allows no more than half of the amplitude of variations with wavelength of two-thirds of the length of series being preserved in resulting indices (Melvin et al., 2007). SPA50 specifies annually varying 50 % frequency cutoff parameter for each year by adding the initial stiffness with ring age. Comparing to SP67, it makes the resulting spline become more flexible in the early years and progressively stiffer in later years (Melvin et al., 2007). All raw ring-width series were divided by the estimated growth trends, and the resulting detrended ring-width series were averaged to generate the standard (STD) chronologies using the bi-weight robust mean method (Fig. S2). Since the traditionally fitted curves may contain low-frequency climatic signals known as “trend distortion” problem; Melvin and Briffa, 2008), the signal-free (SSF) method was introduced to create a fitted growth curve without climatic signals by dividing the raw ring-width series by the STD chronology by means of iterations (Melvin and Briffa, 2008). Therefore, we also developed SSF chronologies for climate analysis (Fig. S3). Following the methods described in Osborn et al. (1997), the variance of each chronology was stabilized to minimize the effects of sampling depth. The temporal extension for all width chronologies in Baiyunshan and Longchiman covers the periods 1841–2005 and 1850–2005, respectively. All the above processes were performed using the program RCSigFree Version 45_v2b (Melvin and Briffa, 2008; <http://www.ldeo.columbia.edu/tree-ring-laboratory/resources/software>). Since the number of cores per tree in our study was unequal, the signal of each chronology was estimated using the effective chronology signal ($Rbar_{eff}$) which incorporates the effective number of cores, within- and between-tree signals (Briffa and Jones, 1990). Besides, the expressed population signal (EPS), a function of $Rbar_{eff}$ and the number of trees, was applied to evaluate how well the sample chronology represents a theoretical chronology (Briffa and Jones, 1990; Wigley et al., 1984). The running $Rbar_{eff}$ and EPS for each chronology were

删除了: Fig. S1

删除了: , and the transition can occur in mid-July in Beijing (39.9° N, 116.3° E; Zhang et al., 1982)

删除了: Due to

删除了: discriminated

删除了: discern

删除了: In order t

删除了: They

删除了: together

删除了: smoothed

删除了: In comparison with

删除了: the

删除了: , which is termed

删除了: (

删除了: is

删除了: the

删除了: free of

删除了: the

删除了: were also developed

删除了: The

删除了: according to the methods described in Osborn et al. (1997)

删除了: are

删除了: with

删除了: are

删除了: qual

删除了: by

删除了: used

删除了: stimate

删除了: the

calculated over a 51-year window with a 50-year overlap using the function “rwi.stats.running” in R package “dplr” version 1.6.9 (Bunn et al., 2018). The minimum number of common years in any pair of ring-width series required for their correlation was set to 30 (Briffa and Jones, 1990). The reliable period for each chronology was determined based on the widely adopted EPS threshold value of 0.85 (Wigley et al., 1984).

删除了: generally accepted

5 The width chronologies from the two sampling sites show high degree of coherence as evidenced by their significant positive correlations ($p < 0.001$) during their common period 1850–2005 (Table S1). Moreover, the positive correlations remain significant ($p < 0.001$) after removing the influence of autocorrelations and linear trends from the tree-ring data (Table S1). These indicate that the two sites share common climatic signals. Therefore, we pooled all raw ring-width series from the two sites, and developed composite STD and SSF chronologies for EWW, LWW and TRW using the three detrending methods as described above (Fig. S4). Statistics for each chronology including the starting year when $EPS \geq 0.85$, standard deviation, mean sensitivity and first-order correlation coefficient (AR1) are shown in Table S2. In addition, several statistics were calculated to assess the degree of similarity among the detrended ring-width series over the common period 1915–2005 (Table S3). These statistics are variance explained by the first eigenvector (Var_{pe1}), R_{bareff} , signal-to-noise ratio (SNR), and EPS (Briffa and Jones, 1990; Trouet et al., 2006).

删除了: is

删除了: s

删除了: signal

15 2.4 Climate data

Monthly mean maximum (Tmax), minimum (Tmin) and mean temperature (Tmean), and monthly total precipitation (Pre) were gathered from four nearby meteorological stations (Table 1; Fig. 1b). These climate data were obtained from the China Meteorological Administration. Regional temperature values were calculated by averaging the temperature time series from the four stations over their common period 1957–2005. Regional precipitation series were calculated by firstly deriving the regional averages in terms of percentages, then multiplying the regional mean to transform the resulting series back to millimetre units (Jones and Hulme, 1996). The self-calibrated PDSI (scPDSI) and SPEI were also chosen as hydroclimatic factors. Here we used the scPDSI instead of PDSI because it has solved the PDSI problems in spatial comparisons by calculating the duration factors (weighting coefficients for the current moisture anomaly and the previous drought severity) based on the characteristics of the climate at a given location (Wells et al., 2004). The regional scPDSI was calculated by averaging the CRU (Climate Research Unit) scPDSI grids (van der Schrier et al., 2013) over the area between 32° N to 34.5° N and 111° E to 112° E (Fig. 1b) where the meteorological stations utilized by CRU dataset were concentrated (Fig. S5; Table S4). The time span of scPDSI was selected as 1953–2005, because the stations used by CRU have a common period starting from July 1952 (Table S4). The SPEI has multi-timescales (Vicente-Serrano et al., 2010). To evaluate the influence of SPEI on monthly, seasonal and annual timescales, we calculated the regional SPEI on three timescales (1-month, 3-month and 12-month) using the R package “SPEI” version 1.7 (Beguiría and Vicente-Serrano, 2017). The climatic factors used in SPEI calculation were regional Tmax, Tmin and Pre, which were derived from the four stations mentioned in Table 1. The time span of SPEI is 1957–2005.

删除了: selected

删除了: directly

删除了: i

删除了: was produced

删除了: the

删除了: Therefore

删除了: at

删除了: 2

删除了: included

In order to validate the reconstruction, we compared it with several hydroclimate time series and historical document records (Table 2). They were (1) the June–August PDSI from the No. 370 grid point of the Monsoon Asia Drought Atlas (MADA) at 33.75° N, 111.25° E over the period 1868–2005 (PDSI_{Cook}; Cook et al., 2010); (2) the dryness/wetness index (DWI) from the grid point at 33.75° N, 111.25° E over the period 1868–2000 (DWI_{Yang}; Yang et al., 2013); (3) reconstructed April–June precipitation based on TRW in Mount Hua over the period 1868–2005 (Pre_{Chen}; Chen et al., 2016b); and (4) drought/wet events recorded in historical documents over the period 1868–2005 (He, 1980; Wen, 2006). The DWI dataset was reconstructed from the historical documents and modern instrumental May–September precipitation in 120 sites over China (Chinese Academy of Meteorological Sciences, 1981). The dataset classified the degree of dryness and wetness into five grades: very wet (grade 1), wet (grade 2), normal (grade 3), dry (grade 4), and very dry (grade 5). Yang et al. (2013) has interpolated the DWI dataset into 2.5° latitude/longitude grid cells.

The EASM circulation was represented using a newly defined EASMI based on the 200 hPa zonal wind anomalies which was less affected by complex weather processes near the surface (Zhao et al., 2015). It was computed using:
$$\text{EASMI} = \text{Nor}[u(2.5^\circ - 10^\circ \text{ N}, 105^\circ - 140^\circ \text{ E}) - u(17.5^\circ - 22.5^\circ \text{ N}, 105^\circ - 140^\circ \text{ E}) + u(30^\circ - 37.5^\circ \text{ N}, 105^\circ - 140^\circ \text{ E})] \quad (1)$$
where Nor and u are standardization and mean 200 hPa zonal wind, respectively. To understand the possible impacts of local precipitation and temperature (32°–34.5° N and 111°–112° E) on the relationship between the scPDSI and EASMI, the precipitation and temperature data were extracted from the gridded precipitation dataset Global Precipitation Climatology Centre Version 7 (GPCC v7; Schneider et al., 2015), and gridded temperature dataset Climatic Research Unit Time-Series Version 4.01 (CRU TS 4.01; Harris et al., 2014), respectively. The gridded dataset can represent the variations of precipitation and temperature over East China in the 20th century (Wang and Wang, 2017; Wen et al., 2006).

2.5 Statistical methods

To investigate the climate response of different tree-ring parameters (EWW, LWW, and TRW), we first calculated the Pearson correlation coefficients of the STD and SSF tree-ring width chronologies using monthly climate time series. The time window for the correlation analysis spanned from January of two years before tree-ring formation to October of the current growth year. Next, correlations were calculated between the prewhitened and linearly detrended chronologies and climate time series in order to evaluate the possible effects of autocorrelations and secular trends. The prewhitening procedure was performed using the “ar” function in R package “stats” version 3.5.1 (R Core Team, 2018). The appropriate autoregressive order was automatically determined by the Akaike Information Criterion (Akaike, 1974). The linear detrending procedure was performed based on the “detrend” function in Matlab R2016a (The MathWorks, Inc., 2016). To find the strongest climate-growth relationship, we analyzed the response of different tree-ring parameters to multi-month averaged scPDSI (which had the stronger impacts on tree-growth than other climatic factors; see the results for details). Finally, we adopted the wavelet coherence method (Grinsted et al., 2004) to test the temporal stability and possible lags of the climate-growth relationship on different frequency domains.

删除了:),

删除了: including

删除了:),

删除了:),

删除了:),

删除了: were

删除了: by

删除了: as Equation (1)

删除了: represent

删除了: during

删除了: ly

删除了: with

删除了: earlier

删除了: Secondly

删除了: run with

删除了: in

删除了: with the “detrend” function

删除了: Then,

删除了: to find the strongest climate-growth relationship.

删除了: used

A simple linear regression model was applied to establish the transfer function using May–July (MJJ) scPDSI as the **predictant**, and the NELR based EWW STD chronology as the predictor (which had the strongest relationship; see the results for detail) over the period 1953–2005. Temporal stability of the model was tested by splitting the MJJ scPDSI into two sub-periods (1953–1979 and 1979–2005) for calibration and verification. **In the process, some statistics (including correlation coefficient**
 5 **(r), explained variance (R^2), reduction of error (RE), coefficient of efficiency (CE), and the sign-test) were applied** (Meko and Graybill, 1995). Meanwhile, the possible autocorrelation and trend contained in the regression residuals were evaluated using the Durbin-Watson test (DW ; Durbin and Watson, 1950) **using** the “dwtest” function in R package “Lmtest” version 0.9-36 (Zeileis and Hothorn, 2002), and the two-sided Cox and Stuart trend test (CS ; Cox and Stuart, 1955) **using** the R package “snpur” version 1.0 (Qiu, 2014), respectively. A DW value of 2 means no first order autocorrelation in the residuals, whereas
 10 values larger (less) than 2 **indicate** for negative (positive) autocorrelation. The DW test has the null hypothesis that the autocorrelation of the residuals is 0. The two-sided CS trend test has the null hypothesis that there is no monotonic trend in the residuals. The variance of the MJJ scPDSI reconstruction was adjusted to match the variance of instrumental MJJ scPDSI during the calibration period using Equation (2),

$$\text{Adj_Rec}_i = \frac{(\text{Rec}_i - \overline{\text{Rec}_{\text{cal}}})}{\sigma(\text{Rec}_{\text{cal}})} \times \sigma(\text{Ins}_{\text{cal}}) + \overline{\text{Ins}_{\text{cal}}} \quad (2)$$

15 where, the Rec_i and Adj_Rec_i **are** the reconstructed value and its variance adjusted value for a specific year i , **respectively**. The $\overline{\text{Rec}_{\text{cal}}}$ and $\overline{\text{Ins}_{\text{cal}}}$ **are** the arithmetic mean of the reconstructed and instrumental values during the calibration period (it is 1953–2005 in this study), **respectively**. The $\sigma(\text{Rec}_{\text{cal}})$ and $\sigma(\text{Ins}_{\text{cal}})$ are the corresponding standard deviations.

To evaluate the spatial representativeness of our reconstruction, spatial correlations were calculated between the reconstructed MJJ scPDSI and CRU scPDSI 3.25 dataset (van der Schrier et al., 2013) using the KNMI Climate Explorer
 20 (<http://climexp.knmi.nl/start.cgi>). **For comparison purpose, all** the hydroclimatic reconstructions were divided into interannual (< 10 years), and decadal and longer-term components (> 10 years), **respectively**. **Decadal and longer frequency** components were derived by lowpass filtering **of** the original reconstructions using the the adaptive 10 point “Butterworth” low-pass filter at 0.1 cut-off frequency (Mann, 2008). **Interannual frequency** components were obtained by subtracting the decadal and longer-term components from the original reconstructions. The low-pass filtering technique **is capable to preserve** trends near time
 25 series boundaries (Mann, 2008).

Following the definition of Zhao et al. (2015), **we calculated the MJJ EASMI** using the 200 hPa zonal wind dataset. **The dataset covering the period 1868–2005 was** obtained from the National Oceanic and Atmospheric Administration–Cooperative Institute for Research in Environmental Sciences Twentieth Century Reanalysis V2c (NOAA-20C; Compo et al., 2011). **The**
 30 **relationship between EASMI and our reconstruction was firstly evaluated using the wavelet coherence method** (Grinsted et al., 2004). **To explore the connections of precipitation and temperature with scPDSI and EASMI,** 21-year moving window correlation analyses were **conducted** between the decadal-filtered MJJ EASMI, reconstructed scPDSI, **local precipitation and temperature**. Moreover, empirical orthogonal function (EOF) analysis and spatial correlation analysis were performed to assess the impacts of the changed leading EASM mode on the relationship between decadal-filtered EASMI and local precipitation.

删除了: predictant

删除了: using the following

删除了: :

删除了: with

删除了: Hothorn et al., 2018

删除了: with

删除了: are indicative

删除了: indicate

删除了: indicate

删除了: S

删除了: to investigate the spatial representativeness of our reconstruction. All

删除了: for comparison,

删除了: The d

删除了: Then, the i

删除了: has a good ability in preserving

删除了: We calculated the MJJ EASMI according to

删除了: which were

删除了:)

删除了: over the period 1868–2005

删除了: In addition,

删除了: calculated

删除了: and

删除了: to explore the connections of precipitation with scPDSI and EASMI...

The filtering procedure was conducted using the “Butterworth” low-pass filter (Mann, 2008) as mentioned above. The filtering, EOF and correlation analyses were performed in Matlab R2016a (The MathWorks, [Inc.](#), 2016) and the plots were drawn with Surfer 10 (Golden Software, [LCC](#), 2011).

The significance tests for all observed correlation coefficients were conducted using Monte Carlo method (Efron and Tibshirani, 1986). In detail, modelled time series with the same structure as the original series were produced [in accordance to](#) the frequency domain method of Ebisuzaki (1997). Then, correlation coefficients were computed between the modelled time series. The above processes were repeated 1000 times to obtain 1000 modelled correlation coefficients. The significance threshold was estimated based on the probability distribution of the modelled 1000 correlation coefficients. The procedure was performed using the algorithms of Macias-Fauria et al. (2012).

10 3 Results and Discussion

3.1 Stronger hydroclimatic signals derived from EWW

[The](#) EWW chronologies generated using different detrending and standardization methods were significantly negatively correlated with Tmax, Tmean during May–June, and significantly positively correlated with [precipitation](#) in May (Fig. 3). [By relating to](#) drought indices, all EWW chronologies were significantly positively correlated with the 1-month SPEI in May, 3-month SPEI during May–June, 12-month SPEI during May–October, and scPDSI during April–October. [Particularly](#), EWW showed a much longer-term response to the multi-month SPEI and scPDSI than to precipitation after May. This may be because the summer temperatures [affected](#) the soil water status as reflected by their negative correlations with EWW. Besides, soil has a memory effect [for](#) previous drought conditions, and this effect [is](#) considered [in](#) the multi-month SPEI and scPDSI (Vicente-Serrano et al., 2010; Dai, 2011). The scPDSI had higher correlation with tree-ring width than the SPEI. This indicates that the scPDSI [is more suitable for](#) monitoring the influence of soil moisture status on tree growth [at](#) our sampling sites, [however](#) the reasons [for this](#) remain unknown [at the moment](#). [The](#) significant correlations between EWW and drought indices during autumn should not be regarded as a real drought impact, as the earlywood growth would terminate in the mid- and late-growing season (Larson, 1969). For LWW, during the current growing season, the highest correlation was found between the NELR based LWW STD and July scPDSI ($r = 0.37$, $p < 0.01$). [However](#), [this correlation](#) was much lower than that [between the](#) NELR based EWW STD and the July scPDSI ($r = 0.62$, $p < 0.01$), indicating that LWW [was](#) less [sensitive](#) to the scPDSI. TRW generally exhibited [a](#) similar climate response as EWW but with relatively lower correlations. Taking the NELR based STD chronologies as an example, the correlation coefficients between TRW and the monthly scPDSI from May to July were 0.59 ($p < 0.01$), 0.58 ($p < 0.01$) [and](#) 0.58 ($p < 0.01$), respectively. However, for EWW, [these](#) correlation coefficients were 0.66 ($p < 0.01$), 0.66 ($p < 0.01$) and 0.62 ($p < 0.01$), [respectively](#). [Similar](#) response patterns were also revealed by the correlation coefficients between the prewhitened and linearly detrended series (Fig. 4), indicating that autocorrelations and secular trends in the tree-ring width chronologies and climate time series [had](#) limited effects on the relationships [with climate](#).

删除了: according to

删除了: As shown in Fig. 3, the

删除了: ,

删除了: Pre

删除了: In terms of the

删除了: ,

删除了: ,

删除了: ,

删除了: It can be found that

删除了: still

删除了: on

删除了: was

删除了: by

删除了: s

删除了: has a better ability

删除了: than the SPEI in

删除了: in

删除了: and

删除了: However, t

删除了: found

删除了:),

删除了: which

删除了: found

删除了: had

删除了: sensitivity

删除了: the

删除了: ,

删除了: The above

删除了: ve

Significant climate-growth relationships were also observed with months prior to the current growing season. For example, most of EWW and LWW chronologies exhibited negative response to Tmax and Tmean during the late summer and early autumn of the last year (Figs. 3 and 4). High temperatures in the late growing season of last year may enhance soil water evaporation, thus inducing moisture stress and limiting the accumulation of photosynthetic products available for the next

5 year's tree-growth (Peng et al., 2014). The influence of moisture status prior to the current growing season is also reflected by the significant positive correlations between LWW and drought indices from September of two years earlier to May of the previous year. However, EWW had lower correlations with these monthly drought indices. A plausible explanation may be that the interannual variations of EWW were mainly contributed by the moisture status of the growth year. Since the impacts of scPDSI on tree growth can last for several months, we analyzed the responses of various tree-ring width

10 parameters to the multi-month averaged scPDSI. The strongest climate-growth relationship was found between the NELR based EWW STD chronology and the MJJ scPDSI ($r = 0.707$; $p < 0.01$; Fig. S6). Meanwhile, correlation coefficients derived from the methods SP67 and SPA50 were 0.67 ($p < 0.01$) and 0.68 ($p < 0.01$), respectively, which were lower than those based the on NELR method (Fig. S6). This may be because the downward trend in MJJ scPDSI was better preserved using the NELR detrending method (Fig. S7). In addition, the correlation coefficient between the NELR based EWW SSF chronology and the

15 MJJ scPDSI was 0.705 ($p < 0.01$), which was quite close to that using the traditional STD method, indicating that the effects of so-called "trend distortion" in our tree-ring series were small. We further tested the temporal stability and possible lags (leads) in the relationships between NELR based STD chronologies and the MJJ scPDSI on different frequency domains (Fig. 5). EWW generally has high degrees of coherence with the MJJ scPDSI on all timescales (2- to 18-year), except for the periodicities between 3.5- and 6.5-year. By contrast, LWW only varied

20 in-phase with the MJJ scPDSI, but with some lags during the period from the 1970s to the 1990s on the timescales shorter than 12 years. Moreover, LWW was inversely correlated with the MJJ scPDSI during the 1960s in the periodicities of 4- to 6-year. TRW showed an unstable relationship and certain lags to the MJJ scPDSI in the periodicities of 6- to 11-year. Therefore, it can be concluded that EWW has more stable relationships with the MJJ scPDSI than LWW and TRW. Previous studies based on TRW demonstrated that moisture status of the current growing season could strongly affect the

25 radial growth of *P. tabulaeformis* (e.g., Cai and Liu, 2013; Cai et al., 2014; Cai et al., 2015; Chen et al., 2014; Fang et al., 2010a; Fang et al., 2012b; Li et al., 2007; Liang et al., 2007; Liu et al., 2017; Song and Liu, 2011; Sun et al., 2012). Fast radial growth of *P. tabulaeformis* usually occurs during the early growing season (Liang et al., 2009; Shi et al., 2008; Zeng et al., 2018). Increased water deficiency due to the rising temperature and inadequate rainfall in the early growing season, induces water stress, suppressing cell division and expansion (Fritts, 1976), and resulting in the formation of narrow earlywood bands.

30 The reduced sensitivity of LWW to the moisture status of the current growing season may be due to that ample water supply in the rainy season (July–August; Fig. 2). TRW and EWW shared similar climatic response. This is because EWW represents the majority of TRW (on average, the portion of EWW of TRW accounts for 65.8%). However, since TRW is also contributed by LWW, the response of TRW to moisture status in the current growing season was somewhat weaker than EWW.

删除了: -

删除了: This may be ascribed that

删除了: h

删除了: thus

删除了: ing

删除了: moisture

删除了:

删除了: -

删除了: analysed

删除了: that

删除了: ere

删除了: limited

删除了: It can be found that

删除了: showed

删除了: Different from EWW,

删除了: lower

删除了: -

删除了: on

删除了: on

删除了: the most

删除了: has evidenced

删除了: 2

删除了: happens

删除了: in

删除了: could

删除了: thus

删除了: less

删除了: ascribed

删除了: the moisture restrictions on tree growth was alleviated

删除了: Meanwhile

删除了: t

删除了: he response sensitivity of TRW to moisture status of the current growing season was not as strong as EWW, although they shared a similar climatic response pattern because EWW represents the majority of TRW (on average, the portion of EWW of TRW accounts for 65.8%)...

3.2 MJJ scPDSI reconstruction using NELR based EWW STD chronology

From above analyses, we identified the MJJ scPDSI as the target for hydroclimate reconstruction, and the NELR based EWW STD chronology as the predictor (Fig. 6a). The transfer function was estimated using a simple linear regression model, as expressed below:

$$\text{MJJ scPDSI} = 4.74\text{EWW} - 4.32; (R^2 = 0.5, n = 53, p < 0.001), \quad (3)$$

The model explained 50 % of the actual MJJ scPDSI variance over the period 1953–2005. The calibration-verification tests revealed that r , R^2 and the sign-test were significant at the 0.01 level, and that RE and CE values were positive (Table 3). In addition, the p -value generated from DW and CS tests were above 0.05, indicating that there were neither autocorrelation nor long-term trends in the regression residuals (Table 3; Fig. 6b). All test results confirmed that the model is valid (Cook et al., 1999; Fritts, 1976).

Based on Equation (3), we reconstructed MJJ scPDSI of the study region back to 1868 (Fig. 6c). We adjusted the variance of the reconstruction to match the variance of instrumental MJJ scPDSI during the calibration period (1953–2005). Spatial correlation analysis indicated that the reconstruction most strongly represents Central China, including the western part of Henan, northern part of Hubei, and southern part of Shaanxi provinces (Fig. 1a).

3.3 Comparing the reconstructed MJJ scPDSI with other climate reconstructions and historical records

On the interannual timescale (Fig. 7a–c), our reconstruction is significantly correlated with the $\text{PDSI}_{\text{Cook}}$ ($r = 0.37$; $p < 0.01$; 1868–2005), and Pre_{Chen} ($r = 0.52$; $p < 0.01$; 1868–2005). On the decadal and longer timescales, our reconstruction is significantly correlated with all other reconstructions from the study region (Fig. 7e and f). The common drought periods occurring in the 1870s and the 1920s in North and West China (Cai et al., 2014; Chen et al., 2014; Fang et al., 2012a; Kang et al., 2013; Liang et al., 2006; Liu et al., 2017; Zhang et al., 2017) were also reflected in our reconstruction.

However, it should be noted that our reconstruction has also some mismatches with others. On the interannual timescale, our reconstruction is not significantly correlated with the DWI_{Yang} over the whole period 1868–2000 ($r = -0.06$; $p = 0.64$; Fig. 7b).

This is probably due to the limited ability of historical documents to capture high-frequency climatic variations (Zheng et al., 2014). On the decadal and longer timescales, our reconstruction varied out-of-phase with $\text{PDSI}_{\text{Cook}}$ during the period from the late 1940s to the early 1960s (Fig. 7d). It was only weakly correlated with DWI_{Yang} after the 1940s (Fig. 7e), and led Pre_{Chen} during the period of 1900s–1930s (Fig. 7f). The might be due to several reasons. Firstly, the reconstructions focused on different target seasons (June–August for $\text{PDSI}_{\text{Cook}}$, May–September for DWI_{Yang} , and April–June for Pre_{Chen} which is before the rainy season). Secondly, the DWI_{Yang} after the 1940s was calculated using instrumental May–September precipitation and the chronology of Chen et al. (2016b) also reflects precipitation, while the scPDSI is influenced not only by precipitation but also temperature and previous drought conditions. Thirdly, in the MADA network includes only a limited number of tree-ring sites in our study region, which may cause deviations on the local scale.

删除了: Based

删除了: on the

删除了: selected

删除了: ,

删除了: in Equation (3)

删除了: s

删除了: of

删除了: show

删除了: are

删除了: are

删除了: are

删除了: larger than

删除了: are

删除了: o

删除了: s

删除了: and

删除了: the above model,

删除了: the

删除了: was

删除了: reconstructed

删除了: s

删除了: the

删除了: the

删除了: documents

删除了: s

删除了: s

删除了: –

删除了: occurring

删除了: were reflected in our reconstruction. These two drought periods were frequently observed in North and West China

删除了:

We also compared the dry and wet events derived from our reconstruction with historical records. Following Palmer (1965), the moderately to severely dry (wet) events are defined based on the scPDSI values less than -2 (larger than 2). Interestingly, all dry events and 70 % of the wet events in our reconstruction can be verified by corresponding descriptions in historical records (Table 4). However, there are still some mismatches between our reconstruction and the historical records. For example, no relevant record is found for the year 1983 when an extreme wet event is shown in our reconstruction. Meanwhile, some historical events are not reflected in our reconstruction, such as the wet event in 1963 and the dry event in 1942 (Wen, 2006). In addition, our reconstruction generally demonstrates a wetter condition compared with other series (especially in its early part), and fails to capture the extreme drought years documented in the past (e.g., 1976–1978 and 1914; Wen, 2006). This might be because the low-frequency hydroclimatic variability preserved in EWW was entangled with the declining biological trend, and was partly removed during the detrending process using simple curve fitting methods (Briffa et al., 1996). A possible approach to preserving the low-frequency hydroclimatic signals is to adopt the Regional Curve Standardization (RCS) method (Briffa et al., 1992), but this requires more field work in the future to collect additional tree-ring samples with an even distribution of different age classes (Briffa et al., 1996).

3.4 Connections with EASMI

In general, the reconstructed MJJ scPDSI and EASMI exhibit an in-phase relationship before the 1940s on the decadal and longer timescales (Fig. 8). This in-phase relationship was further verified after conducting a 21-year moving window correlation analysis on the decadal-filtered scPDSI and EASMI (Fig. 9a, b and e). Since EASM directly drives precipitation rather than the scPDSI, we compared the EASMI with the local precipitation (32° N to 34.5° N and 111° E to 112° E). We found that the local precipitation also exhibits similar variations as the scPDSI and EASMI before the 1940s (Fig. 9a–c). Therefore, the in-phase relationship between the decadal-filtered EASMI and scPDSI before the 1940s may be due to the fact that a stronger EASM could enhance local precipitation, thus increasing the soil moisture content. Interestingly, the correlation between the local precipitation and EASMI weakened after the 1940s, and even became negative since the 1970s (Fig. 9e). We attribute this unstable relationship to the variable nature of EASMI. In fact, the EASMI was designed to capture the leading mode of EASM precipitation variability, whose largest loading is in general located at the mei-yu/changma/baiu rainband (Zhao et al., 2015). In other words, the mei-yu/changma/baiu rainfall has the most robust relationship with the EASMI. Whilst the leading pattern of EASM precipitation could change on interdecadal timescale and longer timescales (which is still elusive due to the limited paleo-precipitation record), the unique importance of mei-yu/changma/baiu in EASM most likely remains (Wang et al., 2008). With the changing precipitation pattern of EASM, the precipitation outside of the mei-yu/changma/baiu rainband could be in-phase, out-of-phase and uncorrelated with mei-yu/changma/baiu rainfall (Wang et al., 2008), which would manifest an unstable relationship with EASMI. The EASM experienced an abrupt shift in the late 1970s, which caused a change of the leading mode of EASM precipitation (Wang, 2001; Ding et al., 2008). We demonstrated how this mode change affects the relationship between EASMI and precipitation in the eastern Qinling Mountains. As shown in Fig. 10a, the anomalies of the decadal-filtered MJJ precipitation exhibited similar variations over the Yangtze River basin and Yellow-

删除了: those recorded in
 删除了: document
 删除了: T
 删除了: according to Palmer (1965). It can be found that
 删除了: the
 删除了: documents
 删除了: While,
 删除了: document
 删除了: In addition
 删除了: These mismatches may reflect the uncertainties of historical documents records and tree-ring.
 删除了:

删除了: T
 删除了: in general
 删除了: n
 删除了: It was
 删除了: the
 删除了: . b and
 删除了: induce
 删除了: ed the
 删除了: However, i
 删除了: iton

删除了: Moreover, although
 删除了: can
 删除了: may even much
 删除了: the unique importance of mei-yu/changma/baiu in EASM most likely remains
 删除了: Therefore, due to
 删除了: e of EASM
 删除了: thus
 删除了: manifesting an
 删除了: r

Huaihe River basins during 1901–1978. However, they were divided by the Yangtze River, showing a dipole pattern during 1979–2005 (Fig. 10b). During both periods, the loading centres were located south of Yangtze River basin (27°–30° N), and the decadal-filtered MJJ precipitation in this area was well captured by the designed EASMI as manifested by their significant positive correlations ($p < 0.1$; Fig. 10c, d). On the contrary, the decadal-filtered MJJ precipitation north of Yangtze River

5 (including our sampling sites) varied out-of-phase with that south of Yangtze River basin after the late 1970s, thus being negatively correlated with the EASMI.

The weakened scPDSI-EASMI relationship after the 1940s cannot be solely attributed to the change of the EASM precipitation mode, because the scPDSI also showed a weakened relationship with the local precipitation simultaneously (Fig. 10f). Neither can it be ascribed simply by the fact that the variations of scPDSI became dominated by temperature either, as no enhanced

10 scPDSI-temperature relationship was found (Fig. 10f). This may be because the scPDSI is not a simple formula based on precipitation and temperature, but a complex function incorporating previous drought conditions and current moisture departure (Wells et al., 2004). In addition to precipitation and temperature, the available energy, humidity and wind speed can also affect the scPDSI via controlling evapotranspiration (Sheffield et al., 2012). Therefore, a variety of climate data is required to identify the specific cause for the observed weakened relationship. However, an exact determination of the causing factors

15 is difficult due to the limited existing climate records.

4 Conclusions

Besides TRW, climatic responses of EWW and LWW were explored for the tree-ring samples of *P. tabulaeformis* from the eastern Qinling Mountains, Central China. Regardless of the detrending and standardisation methods used, the resulting EWW chronologies are more sensitive to early summer soil moisture conditions (scPDSI) than LWW and TRW during the instrumental period 1953–2005. The MJJ scPDSI (1868–2005) reconstructed from the NELR based EWW STD chronology captures the past early summer hydroclimatic fluctuations, which is further validated by other proxy-based reconstructions and historical document records from adjacent regions. This indicates that EWW has a great potential to reconstruct early summer hydroclimatic conditions in the study area. Moreover, on the decadal and longer timescales, our EWW-based hydroclimate reconstruction shows a strong in-phase relationship with the EASMI before the 1940s, which may be related to the positive

20 response of the local precipitation to EASM intensity. Our finding differs from results developed at a well-drained site in South China, where strongest moisture signals are contained in LWW of a different tree species (Zhao et al., 2017a, b). Therefore, more EWW and LWW related studies should be conducted to reveal the tree- and site-specific climate signals in humid and semi-humid regions of China.

删除了: ,

删除了: but

删除了: The s

删除了: the

删除了: were the loading centres during both periods,

删除了: over

删除了: ere

删除了: s

删除了: -

删除了: over the

删除了: the

删除了: ,

删除了: ,

删除了: those

删除了: over the

删除了: the

删除了: ,

删除了: It

删除了: cannot

删除了: to

删除了: stably

删除了: In addition to the precipitation and temperature

删除了: While,

删除了: this would be

删除了: due

删除了: the limited climate records

删除了: in

删除了: ed

删除了: were

删除了: with

删除了: that provide a possibility to understand EASM variations at longer time periods beyond the existing meteorological records. tree species different environmental conditions, in humid and semi-humid regions of China, that provides a possibility to understand EASM variations at longer time periods beyond the meteorological records.

Data availability

The reconstructed May–July scPDSI was included in the supplementary material (Table S5). DWI, precipitation reconstruction, and dry/wet events recorded in historical documents are available from corresponding authors or publications. MADA is available from <https://www.ncdc.noaa.gov/paleo-search/study/10435> (Cook et al., 2010). The 200 hPa zonal wind dataset of NOAA-20C is available from https://www.esrl.noaa.gov/psd/data/gridded/data.20thC_ReanV2c.html (Compo et al., 2011). The gridded dataset CRU scPDSI 3.25 is available from <https://crudata.uea.ac.uk/cru/data/drought/> (van der Schrier et al., 2013). The gridded precipitation dataset GPCP v7 is available from https://opendata.dwd.de/climate_environment/GPCP/html/fulldata_v7_doi_download.html (Schneider et al., 2015). The gridded temperature dataset CRU TS 4.01 is available from https://crudata.uea.ac.uk/cru/data/hrg/cru_ts_4.01/cruts.1709081022.v4.01/tmp/ (Harris et al., 2014).

Author contributions

YZ and JS designed the study. JS provided the tree-ring samples. YZ performed tree-ring width measurement, data analyses and interpretation. JS, SS, XS and HL assisted in data interpretation. YZ wrote the first draft of the paper. All authors revised the paper.

15 Competing interests

The authors declare that they have no conflict of interest.

Acknowledgments

The study was supported by the Key R&D Program of China (Grant No. 2016YFA0600503), the National Natural Science Foundation of China (Grant No. 41671193), and the China Scholarship Council (Grant No. 201706190150 and 201806195033).

20 We thank Dr. Feng Chen for providing his reconstructed precipitation data, and Mr. Zhou Yu for his help in tree-ring width measurements. [We would also like to express our gratitude to EditSprings \(https://www.editsprings.com/\) for the expert linguistic services provided.](https://www.editsprings.com/)

References

25 Akaike, H.: A new look at the statistical model identification, IEEE T. Automat. Contr., 19, 716–723, <https://doi.org/10.1109/TAC.1974.1100705>, 1974.
Beguería, S., and Vicente-Serrano, S. M.: [SPEI](https://CRAN.R-project.org/package=SPEI): Calculation of the Standardised Precipitation-Evapotranspiration Index, <https://CRAN.R-project.org/package=SPEI>, r package version 1.7, 2017.

删除了: tree-ring data used in this study

删除了: ar

删除了: e

删除了: available on request (shijf@nju.edu.cn)

删除了: 20c

删除了: and <https://rda.ucar.edu/datasets/ds628.1/>

删除了: .

删除了: R Package version 1.7,

删除了: cran

删除了: r

删除了: web/

删除了: s/

删除了: /index.html

删除了: 2

Briffa, K. R., and Jones, P. D.: Basic chronology statistics and assessment, in: Methods of dendrochronology: Applications in the environmental sciences, edited by: Cook, E. R., and Kairiukstis, L. A., pp. 137–152. Kluwer Academic Publishers, Dordrecht, Netherlands, <http://doi.org/10.1007/978-94-015-7879-0>, 1990.

5 Briffa, K. R., Jones, P. D., Bartholin, T. S., Eckstein, D., Schweingruber, F. H., Karlén, W., Zetterberg, P., and Eronen, M.: Fennoscandian summers from AD 500: temperature changes on short and long timescales, *Clim. Dynam.*, 7, 111–119, <https://doi.org/10.1007/BF00211153>, 1992.

10 Briffa, K. R., Jones, P. D., Schweingruber, F. H., Karlén, W., and Shiyatov, S. G.: Tree-ring variables as proxy-climate indicators: problems with low-frequency signals, in: Climatic variations and forcing mechanisms of the last 2000 years, edited by: Jones, P. D., Bradley, R. S., and Jouzel, J., Springer, Berlin, Heidelberg, 9–41, http://doi.org/10.1007/978-3-642-61113-1_2, 1996.

Bunn, A., Korpela, M., Biondi, F., Campelo, F., Mérian, P., Qeadan, F., Zang, C., Pucha-Cofrep, D., and Wernicke, J.: `dplR`: Dendrochronology Program Library in R, https://CRAN.R-project.org/packages=dplR_r_package_version_1.6.9, 2018.

Cai, Q., and Liu, Y.: Climatic response of Chinese pine and PDSI variability in the middle Taihang Mountains, north China since 1873, *Trees*, 27, 419–427, <https://doi.org/10.1007/s00468-012-0812-6>, 2013.

15 Cai, Q., Liu, Y., Lei, Y., Bao, G., and Sun, B.: Reconstruction of the March–August PDSI since 1703 AD based on tree rings of Chinese pine (*Pinus tabulaeformis* Carr.) in the Lingkong Mountain, southeast Chinese Loess Plateau, *Clim. Past*, 10, 509–521, <https://doi.org/10.5194/cp-10-509-2014>, 2014.

20 Cai, Q., Liu, Y., Liu, H., and Ren, J.: Reconstruction of drought variability in North China and its association with sea surface temperature in the joining area of Asia and Indian–Pacific Ocean, *Palaeogeogr. Palaeoclimatol. Palaeoecol.*, 417, 554–560, <https://doi.org/10.1016/j.palaeo.2014.10.021>, 2015.

Cai, Q., Liu, Y., Liu, H., Sun, C., and Wang, Y.: Growing-season precipitation since 1872 in the coastal area of subtropical southeast China reconstructed from tree rings and its relationship with the East Asian summer monsoon system, *Ecol. Indic.*, 82, 441–450, <https://doi.org/10.1016/j.ecolind.2017.07.012>, 2017.

25 Chen, F., Yuan, Y., Wei, W., Yu, S., Fan, Z., Zhang, R., Zhang, T., and Shang, H.: Tree-ring-based reconstruction of precipitation in the Changling Mountains, China, since A.D.1691, *Int. J. Biometeorol.*, 56, 765–774, <https://doi.org/10.1007/s00484-011-0431-8>, 2012.

Chen, F., Yuan, Y., Zhang, R., and Qin, L.: A tree-ring based drought reconstruction (AD 1760–2010) for the Loess Plateau and its possible driving mechanisms, *Global Planet. Change*, 122, 82–88, <https://doi.org/10.1016/j.gloplacha.2014.08.008>, 2014.

30 Chen, F., Yu, S., Yuan, Y., Wang, H., and Gagen, M.: A tree-ring width based drought reconstruction for southeastern China: links to Pacific Ocean climate variability, *Boreas*, 45, 335–346, <https://doi.org/10.1111/bor.12158>, 2016a.

Chen, F., Zhang, R., Wang, H., Qin, L., and Yuan, Y.: Updated precipitation reconstruction (AD 1482–2012) for Huashan, north-central China, *Theor. Appl. Climatol.*, 123, 723–732, <https://doi.org/10.1007/s00704-015-1387-0>, 2016b.

35 Chen, J., Huang, W., Jin, L., Chen, J., Chen, S., and Chen, F.: A climatological northern boundary index for the East Asian summer monsoon and its interannual variability, *Sci. China Earth Sci.*, 61, 13–22, <https://doi.org/10.1007/s11430-017-9122-x>, 2018.

Chen, X., and Xu, L.: Temperature controls on the spatial pattern of tree phenology in China's temperate zone, *Agr. Forest Meteorol.*, 154–155, 195–202, <https://doi.org/10.1016/j.agrformet.2011.11.006>, 2012.

40 Chinese Academy of Meteorological Sciences, ed.: Yearly charts of dryness/wetness in China for the last 500-year period, China Cartographic Publishing House, Beijing, China, in Chinese, 1981.

Compo, G. P., Whitaker, J. S., Sardeshmukh, P. D., Matsui, N., Allan, R. J., Yin, X., Gleason, B. E., Vose, R. S., Rutledge, G., Bessemoulin, P., et al.: The twentieth century reanalysis project, *Quarterly J. Roy. Meteorol. Soc.*, 137, 1–28, <https://doi.org/10.1002/qj.776>, 2011.

删除了: 137–146.

删除了: Buras, A., Cecile, J., Mudelsee, M., Schulz, M.,

删除了: p

删除了: l

删除了: R package “dplR” version 1.6.9, CRAN,

删除了: cran

删除了: r

删除了: /web

删除了: /

删除了: /index.html

删除了: 2

删除了: Loess

删除了: (E

删除了: s

删除了:)

删除了: (in Chinese)

删除了: Brönnimann, S., Brunet, M., Crouthamel, R. I., Grant, A. N., Groisman, P. Y., Jones, P. D., Kruk, M. C., Kruger, A. C., Marshall, G. J., Mauerer, M., Mok, H. Y., Nordli, Ø., Ross, T. F., Trigo, R. M., Wang, X. L., Woodruff, S. D., and Worley, S. J.

删除了: T

删除了: C

删除了: R

删除了: P

- Cook, E. R., Briffa, K. R., Shiyatov, S. G., and Mazepa, V.: Tree-ring standardization and growth-trend estimation, in: *Methods of dendrochronology: Applications in the environmental sciences*, edited by: Cook, E. R., and Kairiukstis, L. A., pp. 104–123, Kluwer Academic Publishers, Dordrecht, Netherlands, <http://doi.org/10.1007/978-94-015-7879-0>, 1990.
- 5 Cook, E. R., Meko, D. M., Stahle, D. W., and Cleaveland, M. K.: Drought reconstructions for the continental United States, *J. Climate*, 12, 1145–1162, [https://doi.org/10.1175/1520-0442\(1999\)012<1145:DRFTCU>2.0.CO;2](https://doi.org/10.1175/1520-0442(1999)012<1145:DRFTCU>2.0.CO;2), 1999.
- Cook, E. R., Anchukaitis, K. J., Buckley, B. M., D'Arrigo, R. D., Jacoby, G. C., and Wright, W. E.: Asian monsoon failure and megadrought during the last millennium, *Science*, 328, 486–489, <https://doi.org/10.1126/science.1185188>, 2010.
- Cox, D. R., and Stuart, A.: Some quick sign tests for trend in location and dispersion, *Biometrika*, 42, 80–95, <https://doi.org/10.2307/2333424>, 1955.
- 10 Dai, A.: Characteristics and trends in various forms of the Palmer Drought Severity Index during 1900–2008, *J. Geophys. Res.*, 116, D12, <https://doi.org/10.1029/2010JD015541>, 2011.
- Ding, Y., Wang, Z., and Sun, Y.: Inter-decadal variation of the summer precipitation in East China and its association with decreasing Asian summer monsoon. Part I: Observed evidences, *Int. J. Climatol.*, 28, 1139–1161, <https://doi.org/10.1002/joc.1615>, 2008.
- 15 Ding, Y., Sun, Y., Liu, Y., Si, D., Wang, Z., Zhu, Y., Liu, Y., Song, Y., and Zhang, J.: Interdecadal and interannual variabilities of the Asian summer monsoon and its projection of future change, *Chinese J. Atmos. Sci.*, 37, 253–280, <https://doi.org/10.3878/j.issn.1006-9895.2012.12302>, in Chinese, 2013.
- Durbin, J., and Watson, G. S.: Testing for serial correlation in least squares regression: I, *Biometrika*, 37, 409–428 <https://doi.org/10.2307/2332391>, 1950.
- 20 Ebisuzaki, W.: A method to estimate the statistical significance of a correlation when the data are serially correlated, *J. Climate*, 10, 2147–2153, [https://doi.org/10.1175/1520-0442\(1997\)010<2147:AMTETS>2.0.CO;2](https://doi.org/10.1175/1520-0442(1997)010<2147:AMTETS>2.0.CO;2), 1997.
- Efron, B., and Tibshirani, R.: Bootstrap methods for standard errors, confidence intervals, and other measures of statistical accuracy, *Stat. Sci.*, 1, 54–75, <https://www.jstor.org/stable/2245500>, 1986.
- 25 Fan, Z.-X., Bräuning, A., and Cao, K.-F.: Tree-ring based drought reconstruction in the central Hengduan Mountains region (China) since A.D. 1655, *Int. J. Climatol.*, 28, 1879–1887, <https://doi.org/10.1002/joc.1689>, 2008.
- Fang, K., Gou, X., Chen, F., D'Arrigo, R., and Li, J.: Tree-ring based drought reconstruction for the Guiqing Mountain (China): linkages to the Indian and Pacific Oceans, *Int. J. Climatol.*, 30, 1137–1145, <https://doi.org/10.1002/joc.1974>, 2010a.
- Fang, K., Gou, X., Chen, F., Li, J., D'Arrigo, R., Cook, E., Yang, T., and Davi, N.: Reconstructed droughts for the southeastern Tibetan Plateau over the past 568 years and its linkages to the Pacific and Atlantic Ocean climate variability, *Clim. Dynam.*, 35, 577–585, <https://doi.org/10.1007/s00382-009-0636-2>, 2010b.
- 30 Fang, K., Gou, X., Chen, F., Frank, D., Liu, C., Li, J., and Kazmer, M.: Precipitation variability during the past 400 years in the Xiaolong Mountain (central China) inferred from tree rings, *Clim. Dynam.*, 39, 1697–1707, <https://doi.org/10.1007/s00382-012-1371-7>, 2012a.
- Fang, K., Gou, X., Chen, F., Liu, C., Davi, N., Li, J., Zhao, Z., and Li, Y.: Tree-ring based reconstruction of drought variability (1615–2009) in the Kongtong Mountain area, northern China, *Global Planet. Change*, 80–81, 190–197, <https://doi.org/10.1016/j.gloplacha.2011.10.009>, 2012b.
- 35 Fritts, H. C.: *Tree rings and climate*, Academic Press, New York, 1976.
- Golden Software, LLC: Surfer version 10.1.561, <https://www.goldensoftware.com/products/surfer>, 2011.
- 40 Gou, X., Yang, T., Gao, L., Deng, Y., Yang, M., and Chen, F.: A 457-year reconstruction of precipitation in the southeastern Qinghai-Tibet Plateau, China using tree-ring records, *Chinese Sci. Bull.*, 58, 1107–1114, <https://doi.org/10.1007/s11434-012-5539-7>, 2013.

删除了: 104–123.

删除了: 115

删除了: (in Chinese)

删除了: 77

删除了: 567 pp.,

删除了: Golden, Colorado

- Grinsted, A., Moore, J. C., and Jevrejeva, S.: Application of the cross wavelet transform and wavelet coherence to geophysical time series, *Nonlinear Proc. Geoph.*, 11, 561–566, <https://doi.org/10.5194/npg-11-561-2004>, 2004.
- Guan, B. T., Wright, W. E., Chiang, L.-H., and Cook, E. R.: A dry season streamflow reconstruction of the critically endangered Formosan landlocked salmon habitat, *Dendrochronologia*, 52, 152–161, <https://doi.org/10.1016/j.dendro.2018.10.008>, 2018.
- Hansen, K. G., Buckley, B. M., Zottoli, B., D’Arrigo, R. D., Nam, L. C., Van Truong, V., Nguyen, D. T., and Nguyen, H. X.: Discrete seasonal hydroclimate reconstructions over northern Vietnam for the past three and a half centuries, *Climatic Change*, 145, 177–188, <https://doi.org/10.1007/s10584-017-2084-z>, 2017.
- Harris, I., Jones, P. D., Osborn, T. J., and Lister, D. H.: Updated high-resolution grids of monthly climatic observations – the CRU TS3.10 dataset. *Int. J. Climatol.*, 34, 623–642, <https://doi.org/10.1002/joc.3711>, 2014.
- He, H. W.: Guangxu chunian (1876–1879) Huabei de dahanzai (The North China drought famine of the early Guangxu reign (1876–1879)), Chinese University of Hong Kong Press, Hong Kong, [in Chinese](#), 1980.
- Hughes, M. K., Wu, X. D., Shao, X. M., and Garfin, G. M.: A preliminary reconstruction of rainfall in North-Central China since A.D. 1600 from tree-ring density and width, *Quaternary Res.*, 42, 88–99, <https://doi.org/10.1006/qres.1994.1056>, 1994.
- 15 [Jiang, Z., He, J., Li, J., Yang, J., and Wang, J.: Northerly advancement characteristics of the East Asian summer monsoon with its interdecadal variations, *Acta Geographica Sinica*, 61, 675–686 <https://doi.org/10.11821/xb200607001>, in Chinese, 2006.](#)
- Jones, P. D., and Hulme, M.: Calculating regional climatic time series for temperature and precipitation: methods and illustrations, *Int. J. Climatol.*, 16, 361–377, [https://doi.org/10.1002/\(SICI\)1097-0088\(199604\)16:4<361::AID-JOC53>3.0.CO;2-F](https://doi.org/10.1002/(SICI)1097-0088(199604)16:4<361::AID-JOC53>3.0.CO;2-F), 1996.
- 20 Kang, S., Yang, B., Qin, C., Wang, J., Shi, F., and Liu, J.: Extreme drought events in the years 1877–1878, and 1928, in the southeast Qilian Mountains and the air–sea coupling system, *Quatern. Int.*, 283, 85–92, <https://doi.org/10.1016/j.quaint.2012.03.011>, 2013.
- Knapp, P. A., Maxwell, J. T., and Soulé, P. T.: Tropical cyclone rainfall variability in coastal North Carolina derived from longleaf pine (*Pinus palustris* Mill.): AD 1771–2014, *Climatic Change*, 135, 311–323, <https://doi.org/10.1007/s10584-015-1560-6>, 2016.
- 25 Larson, P. R.: Wood formation and the concept of wood quality, Bulletin no. 74, [New Haven, CT: Yale University, School of Forestry](#), pp. 1–54, 1969.
- Lei, Y., Liu, Y., Song, H., and Sun, B.: A wetness index derived from tree-rings in the Mt. Yishan area of China since 1755 AD and its agricultural implications, *Chinese Sci. Bull.*, 59, 3449–3456, <https://doi.org/10.1007/s11434-014-0410-7>, 2014.
- 30 Li, J., Chen, F., Cook, E. R., Gou, X., and Zhang, Y.: Drought reconstruction for north central China from tree rings: the value of the Palmer drought severity index, *Int. J. Climatol.*, 27, 903–909, <https://doi.org/10.1002/joc.1450>, 2007.
- Li, J., Shi, J., Zhang, D. D., Yang, B., Fang, K., and Yue, P. H.: Moisture increase in response to high-altitude warming evidenced by tree-rings on the southeastern Tibetan Plateau, *Clim. Dynam.*, 48, 649–660, <https://doi.org/10.1007/s00382-016-3101-z>, 2017.
- 35 Li, Y., Fang, K., Cao, C., Li, D., Zhou, F., Dong, Z., Zhang, Y., and Gan, Z.: A tree-ring chronology spanning 210 years in the coastal area of southeast China, and its relationship with climate change, *Clim. Res.*, 67, 209–220, <https://doi.org/10.3354/cr01376>, 2016.
- Liang, E., and Eckstein, D.: Light rings in Chinese pine (*Pinus tabulaeformis*) in semiarid areas of north China and their palaeo-climatological potential, *New Phytol.*, 171, 783–791, <https://doi.org/10.1111/j.1469-8137.2006.01775.x>, 2006.
- 40 Liang, E., Liu, X., Yuan, Y., Qin, N., Fang, X., Huang, L., Zhu, H., Wang, L., and Shao, X.: The 1920s drought recorded by tree rings and historical documents in the semi-arid and arid areas of northern China, *Climatic Change*, 79, 403–432, <https://doi.org/10.1007/s10584-006-9082-x>, 2006.

删除了:

删除了: (in Chinese).

删除了: Hothorn, T., Zeileis, A., Farebrother, R. W., Cummins, C., Millo, G., and Mitchell, D.: Testing linear regression models, R package “lmtest” version 0.9-36, CRAN, <https://cran.r-project.org/web/packages/lmtest/index.html>, 2018.

删除了:

删除了: Yale University, New Haven,

删除了: pp.

- Liang, E., Shao, X., Liu, H., and Eckstein, D.: Tree-ring based PDSI reconstruction since AD 1842 in the Ortindag Sand Land, east Inner Mongolia, Chinese Sci. Bull., 52, 2715–2721, <https://doi.org/10.1007/s11434-007-0351-5>, 2007.
- Liang, E., Eckstein, D., and Shao, X.: Seasonal cambial activity of relict Chinese Pine at the northern limit of its natural distribution in North China - [Exploratory](#) results, IAWA J., 30, 371–378, <https://doi.org/10.1163/22941932-90000225>, 2009.
- 5 Liu, H., Shao, X., and Huang, L.: Reconstruction of early-summer drought indices in mid-north region of China after 1500 using tree ring chronologies, Quaternary Sciences, 22, 220–229, [in Chinese](#), 2002.
- Liu, X., Nie, Y., and Wen, F.: Seasonal dynamics of stem radial increment of *Pinus taiwanensis* Hayata and its response to environmental factors in the Lushan Mountains, Southeastern China, Forests, 9, 387, <https://doi.org/10.3390/f9070387>, [2018a](#).
- Liu, Y., Zhang, X., Song, H., Cai, Q., Li, Q., Zhao, B., Liu, H., and Mei, R.: Tree-ring-width-based PDSI reconstruction for central Inner Mongolia, China over the past 333 years, Clim. Dynam., 48, 867–879, <https://doi.org/10.1007/s00382-016-3115-6>, 2017.
- Liu, Y., Song, H., Sun, C., Song, Y., Cai, Q., Liu, R., Lei, Y., and Li, Q.: The 600-mm precipitation isoline distinguishes tree-ring-width responses to climate in China, Natl. Sci. Rev., [6](#), 359–368, <https://doi.org/10.1093/nsr/nwy101>, [2018b](#).
- 15 Macias-Fauria, M., Grinsted, A., Helama, S., and Holopainen, J.: Persistence matters: Estimation of the statistical significance of paleoclimatic reconstruction statistics from autocorrelated time series, Dendrochronologia, 30, 179–187, <https://doi.org/10.1016/j.dendro.2011.08.003>, 2012.
- Mann, M. E.: Smoothing of climate time series revisited, Geophys. Res. Lett., 35, L16708, <https://doi.org/10.1029/2008gl034716>, 2008.
- 20 Meko, D., and Graybill, D. A.: Tree-ring reconstruction of upper Gila River discharge, Water Resour. Bull., 31, 605–616, <https://doi.org/10.1111/j.1752-1688.1995.tb03388.x>, 1995.
- Melvin, T. M., and Briffa, K. R.: A “signal-free” approach to dendroclimatic standardisation, Dendrochronologia, 26, 71–86, <https://doi.org/10.1016/j.dendro.2007.12.001>, 2008.
- Melvin, T. M., Briffa, K. R., Nicolussi, K., and Grabner, M.: Time-varying-response smoothing, Dendrochronologia, 25, 65–69, <https://doi.org/10.1016/j.dendro.2007.01.004>, 2007.
- 25 Osborn, T. J., Briffa, K. R., and Jones, P. D.: Adjusting variance for sample-size in tree-ring chronologies and other regional-mean time series, Dendrochronologia, 15, 89–99, 1997.
- Palmer, W. C., Meteorological drought, [US weather bureau research paper No. 45](#), pp. 1–58, 1965.
- Peng, J., Liu, Y., and Wang, T.: A tree-ring record of 1920's–1940's droughts and mechanism analyses in Henan Province, Acta Ecologica Sinica, 34, 3509–3518, <https://doi.org/10.5846/stxb201306121687>, [in Chinese](#), 2014.
- 30 Qiu, D.: [snpar](#): Supplementary non-parametric statistics methods, <https://CRAN.R-project.org/package=snpar>, [R package version 1.0](#), 2014.
- R Core Team: [R: A Language and Environment for Statistical Computing](#), R Foundation for Statistical Computing, Vienna, Austria, <https://www.R-project.org/>, 2018.
- 35 Schneider, U., Becker, A., Finger, P., Meyer-Christoffer, A., Rudolf, B., and Ziese, M.: GPCC full data monthly product version 7.0 at 0.5°: Monthly land-surface precipitation from rain-gauges built on GTS-based and historic data, Global Precipitation Climatology Centre (GPCC), Berlin, Germany, https://doi.org/10.5676/DWD_GPCC/FD_M_V7_050, 2015.
- Sheffield, J., Wood, E. F., and Roderick, M. L.: Little change in global drought over the past 60 years, Nature, 491, 435–438, <https://doi.org/10.1038/nature11575>, 2012.
- 40 Shi, J.F., Liu, Y., Vaganov, E. V., Li, J. B., and Cai, Q. F.: Statistical and process-based modeling analyses of tree growth response to climate in semi-arid area of north central China: A case study of *Pinus tabulaeformis*, J. Geophys. Res., 113, G01026, <https://doi.org/10.1029/2007JG000547>, 2008.

删除了: exploratory

删除了: (in Chinese)

删除了: 2018a

删除了: 2018b

删除了:

删除了: -

删除了: W

删除了: B

删除了: R

删除了: P

删除了: U.S. Department of Commerce, Washington, D.C.,

删除了: pp.

删除了: (in Chinese)

删除了: R

删除了: “snpar”

删除了: CRAN, <https://cran.r-project.org/web/packages/snpar/index.html>, ...

删除了: l

删除了: e

删除了: s

删除了: c

删除了: package “stats” version 3.5.1, Vienna,

- Shi, J., Li, J., Cook, E. R., Zhang, X., and Lu, H.: Growth response of *Pinus tabulaeformis* to climate along an elevation gradient in the eastern Qinling Mountains, central China, *Clim. Res.*, 53, 157–167, <https://doi.org/10.3354/cr01098>, 2012.
- Shi, J., Lu, H., Li, J., Shi, S., Hou, X., and Li, L.: Tree-ring based February–April precipitation reconstruction for the lower reaches of the Yangtze River, Southeast China, *Global Planet. Change*, 131, 82–88, <https://doi.org/10.1016/j.gloplacha.2015.05.006>, 2015.
- 5 Song, H., and Liu, Y.: PDSI variations at Kongtong Mountain, China, inferred from a 283-year *Pinus tabulaeformis* ring width chronology, *J. Geophys. Res.-Atmos.*, 116, <https://doi.org/10.1029/2011jd016220>, 2011.
- Stahle, D. W., Cleaveland, M. K., Grissino-Mayer, H. D., Griffin, R. D., Fye, F. K., Therrell, M. D., Burnette, D. J., Meko, D. M., and Villanueva Diaz, J.: Cool- and warm-season precipitation reconstructions over western New Mexico, *J. Climate*, 22, 3729–3750, <https://doi.org/10.1175/2008JCLI2752.1>, 2009.
- 10 Sun, J., Liu, Y., Sun, B., and Wang, R.: Tree-ring based PDSI reconstruction since 1853 AD in the source of the Fenhe River Basin, Shanxi province, China, *Sci. China Earth Sci.*, 55, 1847–1854, <https://doi.org/10.1007/s11430-012-4369-4>, 2012.
- Tang, X., Chen, B., Liang, P., and Qian, W.: Definition and features of the north edge of the East Asian summer monsoon, *J. Meteorol. Res.-PRC*, 24, 43–49, 2010.
- 15 The MathWorks, Inc.: MATLAB and Statistics Toolbox Release 2016a, <https://www.mathworks.com>, 2016.
- Trouet, V., Coppin, P., and Beeckman, H.: Annual growth ring patterns in *Brachystegia spiciformis* reveal influence of precipitation on tree growth, *Biotropica*, 38, 375–382, <https://doi.org/10.1111/j.1744-7429.2006.00155.x>, 2006.
- van der Schrier, G., Barichivich, J., Briffa, K. R., and Jones, P. D.: A scPDSI-based global data set of dry and wet spells for 1901–2009, *J. Geophys. Res.-Atmos.*, 118, 4025–4048, <https://doi.org/10.1002/jgrd.50355>, 2013.
- 20 Vicente-Serrano, S. M., Beguería, S., and López-Moreno, J. I.: A multiscalar drought index sensitive to global warming: the standardized precipitation evapotranspiration index, *J. Climate*, 23, 1696–1718, doi:10.1175/2009JCLI2909.1, 2010.
- Wang, B., Wu, Z., Li, J., Liu, J., Chang, C.-P., Ding, Y., and Wu, G.: How to measure the strength of the East Asian summer monsoon, *J. Climate*, 21, 4449–4463, <https://doi.org/10.1175/2008jcli2183.1>, 2008.
- Wang, D., and Wang, A.: Applicability assessment of GPCP and CRU precipitation products in China during 1901 to 2013, *Climatic and Environmental Research*, 22, 446–462, <https://doi.org/10.3878/j.issn.1006-9585.2016.16122>, [in Chinese](#), 2017.
- 25 Wang, H.: The weakening of the Aisan monsoon circulation after the end of 1970’s, *Advances in Atmospheric Sciences*, 18, 376–386, <https://doi.org/10.1007/BF02919316>, 2001.
- Wang, L., Fang, K., Chen, D., Dong, Z., Zhou, F., Li, Y., Zhang, P., Ou, T., Guo, G., Cao, X., and Yu, M.: Intensified variability of the El Niño–Southern Oscillation enhances its modulations on tree growths in southeastern China over the past 218 years, *Int. J. Climatol.*, 38, 5293–5304, <https://doi.org/10.1002/joc.5730>, 2018.
- 30 Wells, N., Goddard, S., and Hayes, M. J.: A self-calibrating Palmer Drought Severity Index, *J. Climate*, 17, 2335–2351, [https://doi.org/10.1175/1520-0442\(2004\)017<2335:ASPDSI>2.0.CO;2](https://doi.org/10.1175/1520-0442(2004)017<2335:ASPDSI>2.0.CO;2), 2004.
- Wen, K., ed.: *Meteorological disasters in China*, China Meteorological Press, Beijing, China, [in Chinese](#), 2006.
- Wen, X.-Y., Wang, S.-W., Zhu, J.-H., and David, V.: An overview of China climate change over the 20th century using UK/UEA/CRU high resolution grid data, *Chinese J. Atmos. Sci.*, 30, 894–903, [in Chinese](#), 2006.
- 35 Wigley, T. M. L., Briffa, K. R., and Jones, P. D.: On the average value of correlated time series, with applications in dendroclimatology and hydrometeorology, *J. Clim. App. Meteorol.*, 23, 201–213, [https://doi.org/10.1175/1520-0450\(1984\)023<0201:otavoc>2.0.co;2](https://doi.org/10.1175/1520-0450(1984)023<0201:otavoc>2.0.co;2), 1984.
- Xu, H. C., Sun, Z. F., Guo, G., and Feng, L.: Geographic distribution of *Pinus tabulaeformis* Carr. and classification of provenance regions, *Scientia Silvae Sinicae*, 17, 258–270, [in Chinese](#), 1981.
- 40

删除了: Natick, Massachusetts

删除了: (in Chinese)

删除了: (

删除了: E

删除了: s

删除了:)

删除了: (in Chinese)

删除了: (in Chinese)

删除了: (in Chinese)

- Yang, F., Shi, F., Kang, S., Wang, S., Xiao, Z., Nakatsuka, T., and Shi, J.: Comparison of the dryness/wetness index in China with the Monsoon Asia Drought Atlas, *Theor. Appl. Climatol.*, 114, 553–566, <https://doi.org/10.1007/s00704-013-0858-4>, 2013.
- 5 [Zeileis, A. and Hothorn, T.: Diagnostic Checking in Regression Relationships, R News, 2, 7-10, https://CRAN.R-project.org/doc/Rnews/, 2002.](https://CRAN.R-project.org/doc/Rnews/)
- Zeng, Q., Rossi, S., and Yang, B.: Effects of age and size on xylem phenology in two conifers of Northwestern China, *Front. Plant. Sci.*, 8, 2264, <https://doi.org/10.3389/fpls.2017.02264>, 2018.
- Zhang, Y., Tian, Q., Guillet, S., and Stoffel, M.: 500-yr. precipitation variability in Southern Taihang Mountains, China, and its linkages to ENSO and PDO, *Climatic Change*, 144, 419–432, <https://doi.org/10.1007/s10584-016-1695-0>, 2017.
- 10 Zhang, Y.-B., Zheng, H.-M., Long, R.-Z., and Yang, B.-C.: Seasonal cambial activity and formation of phloem and xylem in eight forest tree species grown in North China, *Scientia Silvae Sinicae*, 18, 366–379, [in Chinese](#), 1982.
- [Zhao, G., Huang, G., Wu, R., Tao, W., Gong, H., Qu, X., and Hu, K.: A new upper-level circulation index for the East Asian summer monsoon variability, J. Climate, 28, 9977–9996, https://doi.org/10.1175/jcli-d-15-0272.1, 2015.](#)
- 15 Zhao, Y., Shi, J., Shi, S., Wang, B., and Yu, J.: Summer climate implications of tree-ring latewood width: a case study of *Tsuga longibracteata* in South China, *Asian Geographer*, 34, 131–146, <https://doi.org/10.1080/10225706.2017.1377623>, 2017a.
- Zhao, Y., Shi, J., Shi, S., Yu, J., and Lu, H.: Tree-ring latewood width based July–August SPEI reconstruction in South China since 1888 and its possible connection with ENSO, *J. Meteorol. Res.-PRC*, 31, 39–48, <https://doi.org/10.1007/s13351-017-6096-4>, 2017b.
- 20 [Zheng, J., Ge, Q., Hao, Z., Liu, H., Man, Z., Hou, Y., and Fang, X.: Paleoclimatology proxy recorded in historical documents and method for reconstruction on climate change, Quaternary Sciences, 34, 1186–1196, https://doi.org/10.3969/j.issn.1001-7410.2014.06.07, in Chinese, 2014.](#)

删除了: (in Chinese)

删除了: Zheng, J., Ge, Q., Hao, Z., Liu, H., Man, Z., Hou, Y., and Fang, X.: Paleoclimatology proxy recorded in historical documents and method for reconstruction on climate change, *Quaternary Sciences*, 34, 1186–1196, <https://doi.org/10.3969/j.issn.1001-7410.2014.06.07>, 2014 (in Chinese).

Table 1. Characteristics of climate data series used in correlation analyses.

Climate data	Source	Longitude (° E)	Latitude (° N)	Elevation (m a.s.l.)	Temporal cover
Tmax, Tmean,	Luanchuan (LC) meteorological station	111.6	33.8	750.3	1957–2005
Tmin, Pre	Xixia (XX) meteorological station	111.5	33.3	250.3	1957–2005
	Ruyang (RY) meteorological station	112.5	34.2	307.8	1957–2005
	Nanzhao (NZ) meteorological station	112.6	33.6	199.7	1956–2005
scPDSI	CRU scPDSI 3.25 (van der Schrier et al., 2013)	111–112	32–34.5	—	1953–2005
SPEI	Calculated in R using the SPEI package with the monthly maximum and minimum temperature, and total precipitation (Beguería and Vicente-Serrano, 2012)	—	—	—	1957–2005

删除了: .

删除了: Tmax

删除了: , T

删除了: n

删除了: Pre data

Table 2. Long-term hydroclimatic reconstructions and East Asian summer monsoon index (EASMI) selected for comparing with the reconstructed MJJ scPDSI from this study.

Time series	Source	Longitude (° E)	Latitude (° N)	Temporal cover
June–August PDSI	Monsoon Asia Drought Atlas (MADA; Cook et al., 2010)	111.25	33.75	1868–2005
April–June precipitation in Mount Huashan (HS)	Chen et al. (2016b)	110.08	34.47	1868–2005
Dryness/wetness index (DWI)	Yang et al. (2013)	111.25	33.75	1868–2000
EASMI	Calculated using the 200 hPa zonal wind anomalies (NOAA-20C; Compo et al., 2011) according to the definition of Zhao et al. (2015)	—	—	1868–2005

删除了: ion

删除了: ,

删除了: ,

删除了: ,

删除了: 20c

Table 3. Statistics of regression models for split calibration-verification periods.

Calibration period	r	R^2	DW value (p -value)	CS p -value	Verification period	RE	CE	Sign-test
Full period (1953–2005)	0.71**	0.50**	2.03 (0.53)	0.85	—	—	—	—
Early half (1953–1979)	0.68**	0.46**	2.02 (0.49)	1	Late half (1979–2005)	0.53	0.53	22+/5–**
Late half (1979–2005)	0.73**	0.54**	2.02 (0.50)	1	Early half (1953–1979)	0.46	0.45	21+/6–**

** $p < 0.01$; r , Pearson correlation coefficient; R^2 , explained variance; DW , Durbin-Watson test; CS , Cox and Stuart trend test; RE , reduction of error; and CE , coefficient of efficiency.

删除了: for

删除了: of the regression model

Table 4. Moderately to severely dry ($scPDSI \leq -2$) and wet ($scPDSI \geq 2$) events derived from the MJJ scPDSI reconstruction and corresponding descriptions from historical records.

Event type	Year	scPDSI	Description
Dry	1879	-3.61	A mega-drought occurred, caused a great famine over Henan, Shaanxi and other provinces in North China in the early Guangxu reign (1876–1879) ^a
	1900	-2.24	Severe drought from spring to Autumn over Henan and Shaanxi
	1923	-2.28	Drought over Henan and Shaanxi
	1926	-2.33	No harvest at Ruyang (West Henan) due to severe drought
	1929	-2.53	Summer drought over Henan and Shaanxi
	1994	-2.12	Severe drought occurred in April, May and July over west Henan
	1995	-2.10	Intensified drought severity since April 22 over Henan
	2000	-2.94	The drought from February to May was the worst one since 1950 over Henan
Wet	1869	2.31	Flood in summer and autumn over Henan
	1883	2.62	Persistent rainfall in summer at Shanxian and Mianchi (Northwest Henan)
	1885	3.07	Flood in summer at Lingbao and Shanxian (Northwest Henan)
	1894	3.06	Not available
	1895	2.11	Flood of the Qinhe River (Northwest Henan) in summer
	1898	3.77	Severe flood in summer at Lushi (Northwest Henan), Shangnan (Southeast Shaanxi) and Danjiang (Northwest Hubei)
	1905	2.26	Persistent rainfall in spring and summer over Henan

删除了: documents

删除了: has

删除了: r

删除了: is

删除了: over

1906	3.65	Heavy rainfall in summer over Henan
1910	2.05	Flood in summer and autumn over Henan
1911	3.84	Heavy rainfall in summer over Henan
1912	2.01	Heavy rainfall and flood in summer over Nanyang (Southwest Henan)
1933	2.51	Heavy rainfall in summer over Henan and Shaanxi
1934	3.11	Summer rainfall over Henan, South Shaanxi and Northwest Hubei
1936	3.72	Not available
1944	2.38	Flood over Henan; Rainstorm in Zhenan (Southeast Shaanxi) on July 8; The Tianhui Channel (Southeast Shaanxi) was destroyed by flood on May 13
1948	2.81	Wheat loss caused by summer rainfall
1949	2.95	Not available
1973	2.97	Not available
1980	2.07	Rainfall in June was higher than usual for most regions over Henan
1983	4.15	Not available
1984	2.33	From June to September, there were 5 large-scale rainstorms over Henan
1990	2.32	Not available

删除了: is

删除了: are

^a Historical description of the 1879 drought event is cited from He (1980), and others from Wen (2006).

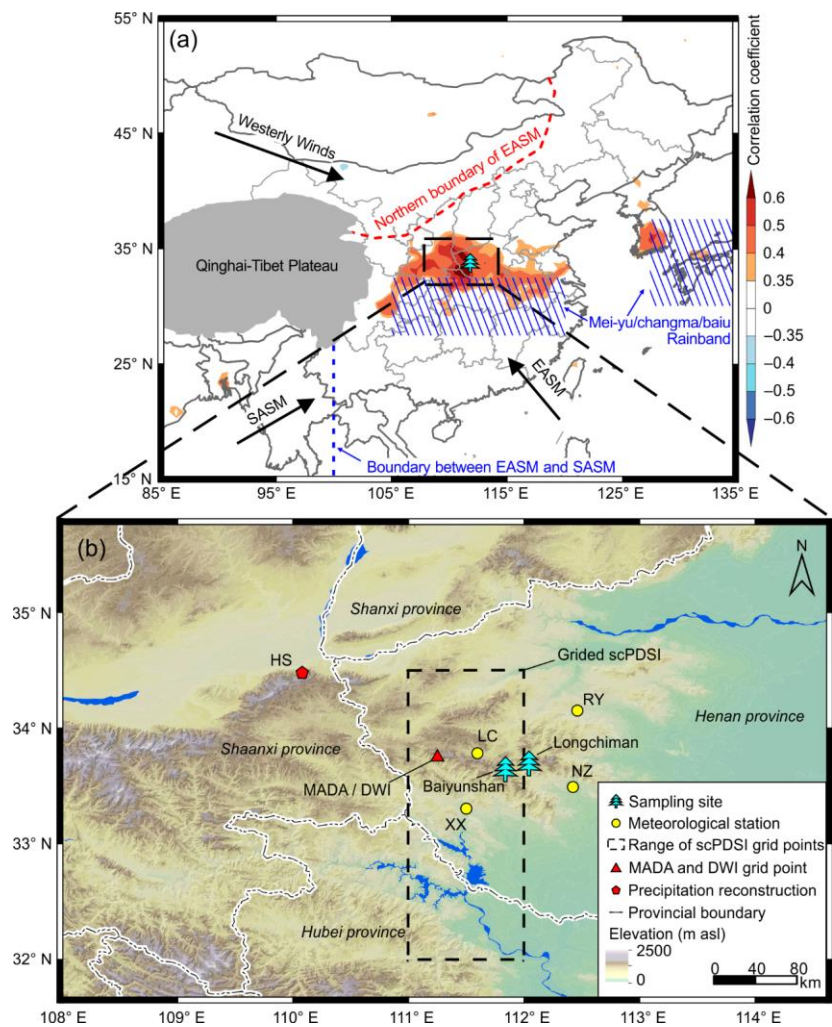


Figure 1. Map of the study region. (a) Location of the sampling site (tree symbol), and the spatial correlations between the May–July (MJJ) scPDSI reconstruction and the gridded scPDSI dataset (van der Schrier et al., 2013) during the period 1953–2005. The color bar indicates the correlation coefficient. The blue dashed line (100° E) indicates the boundary between East

Asian summer monsoon (EASM) and South Asian summer monsoon (SASM; Tang et al., 2010). The red dashed line indicates the northern boundary of EASM (Chen et al., 2018). The blue shaded area represents the mei-yu/changma/baiu rainband (Zhao et al., 2015). **(b)** Partial enlargement of the study region. The circles indicate the locations of the four meteorological stations (LC: Luanchuan, XX: Xixia, RY: Ruyang, and NZ: Nanzhao). The triangle indicates the location of selected grid data from the datasets Monsoon Asia Drought Atlas (MADA; Cook et al., 2010) and Dryness/Wetness Index (DWI; Yang et al., 2013). The pentagon indicates a tree-ring width based precipitation reconstruction in Huashan Mount (HS; Chen et al., 2016b). The dashed rectangle indicates the gridded scPDSI obtained from the gridded scPDSI dataset (van der Schrier et al., 2013).

删除了: .

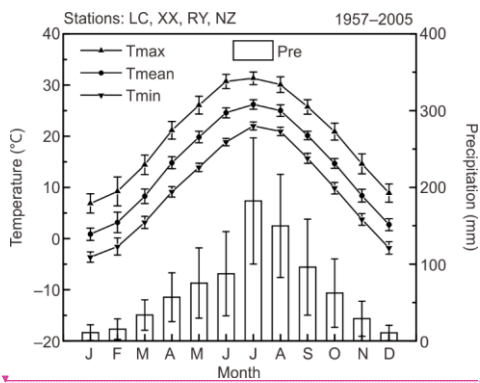
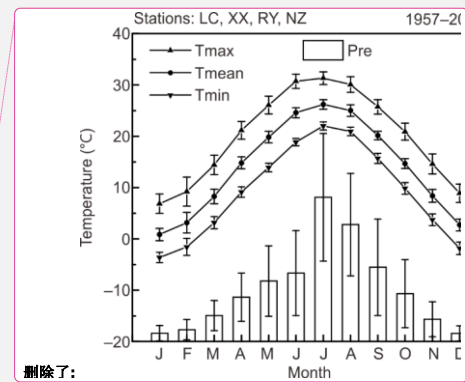


Figure 2. Monthly maximum, mean, minimum temperature (Tmax, Tmean, Tmin), and total precipitation (Pre) averaged from the four selected meteorological stations (LC: Luanchuan, XX: Xixia, RY: Ruyang, and NZ: Nanzhao) during the period 1957–2005. Error bar denotes \pm one standard deviation.



删除了:

删除了: LC, XX, RY, NZ

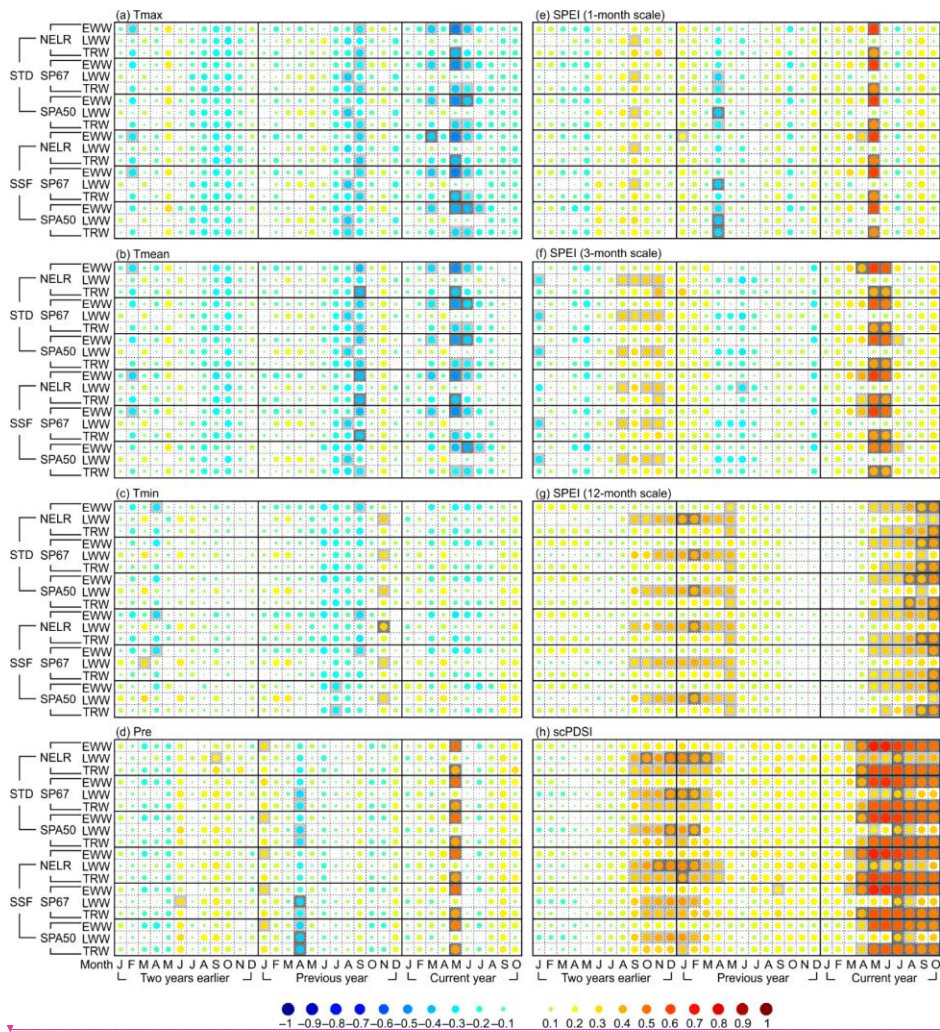
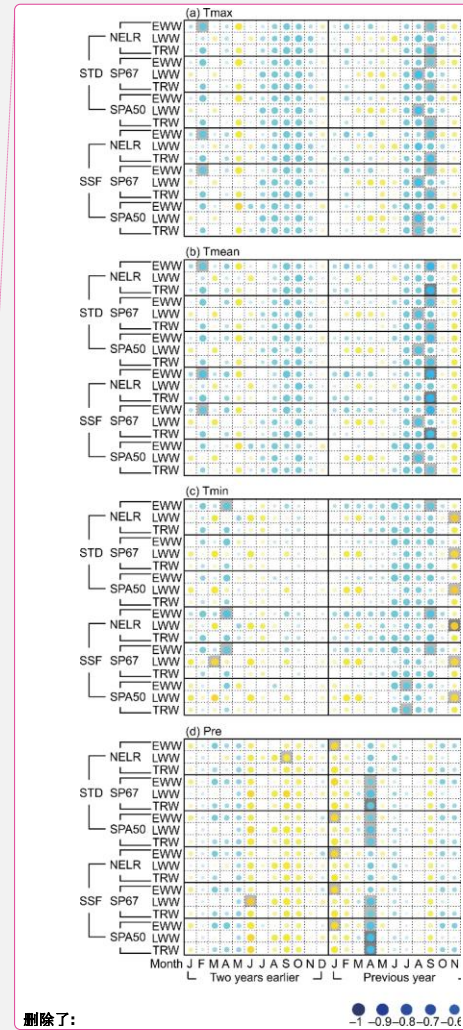


Figure 3. Matrix plots for the correlation coefficients between tree-ring width chronologies and monthly climate time series from January of two years earlier to October of the current year. The climatic factors are monthly (a) maximum temperature



删除了:

(Tmax), (b) mean temperature (Tmean), (c) minimum temperature (Tmin), (d) total precipitation (Pre), (e) SPEI of 1-month scale, (f) SPEI of 3-month scale, (g) SPEI of 12-month scale, and (h) scPDSI. EWW, LWW, and TRW represent the earlywood width, latewood width, and total tree-ring width, respectively. The correlation analyses were conducted for the period 1953–2005 for the scPDSI, and for 1957–2005 for the other climatic factors. NELR, SP67, and SPA50 indicate the three detrending methods: (1) negative exponential functions combined with linear regression with negative (or zero) slope (NELR), (2) cubic smoothing splines with a 50 % frequency cutoff of 67 % of the series length (SP67), and (3) age-dependent splines with an initial stiffness of 50 years (SPA50). STD and SSF indicate the two standardization methods “standard” and “signal-free”, respectively. The correlation coefficients are reflected by the colorful and different-size circles, which can be referred to the color bar as shown at the bottom of the figure. The squares filled with light and dark gray color indicate that the correlation coefficients are statistically significant at the 0.05 and 0.01 level, which are tested using the Monte Carlo method (Efron and Tibshirani, 1986; Macias-Fauria et al., 2012).

删除了: indicate

删除了: during

删除了: together

删除了: ed

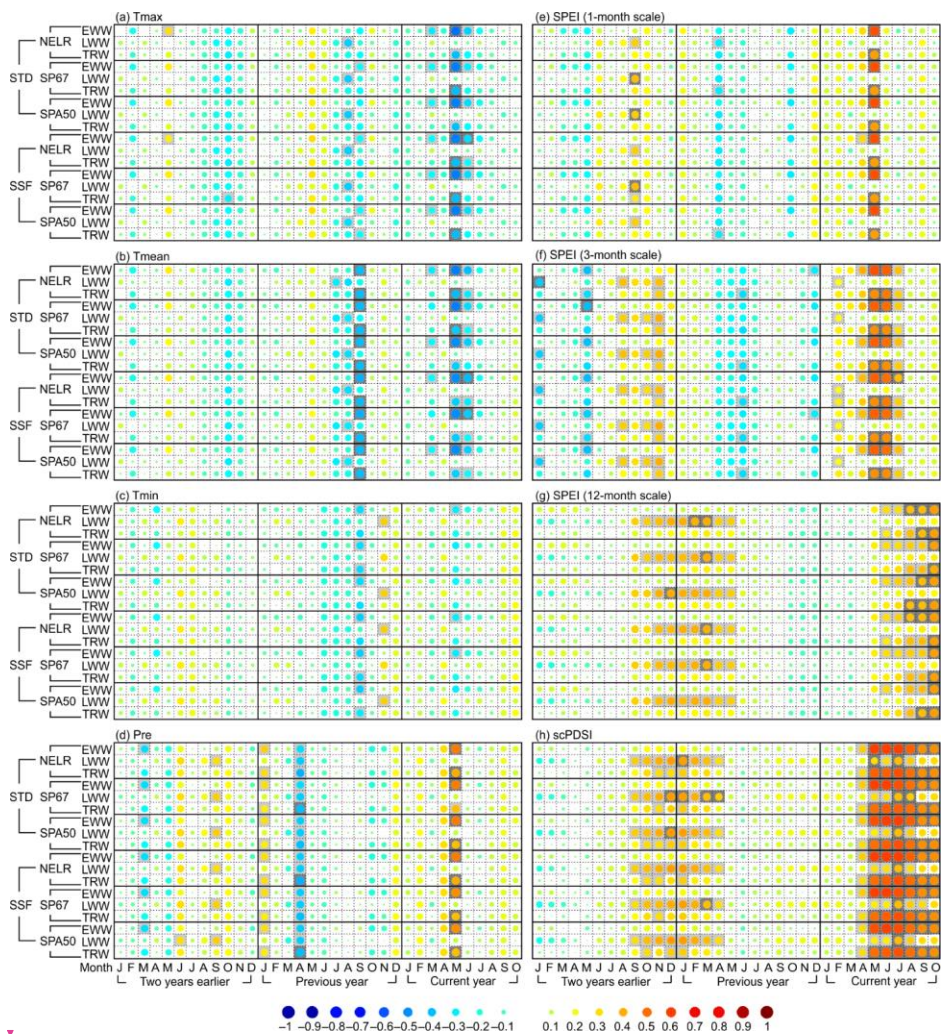
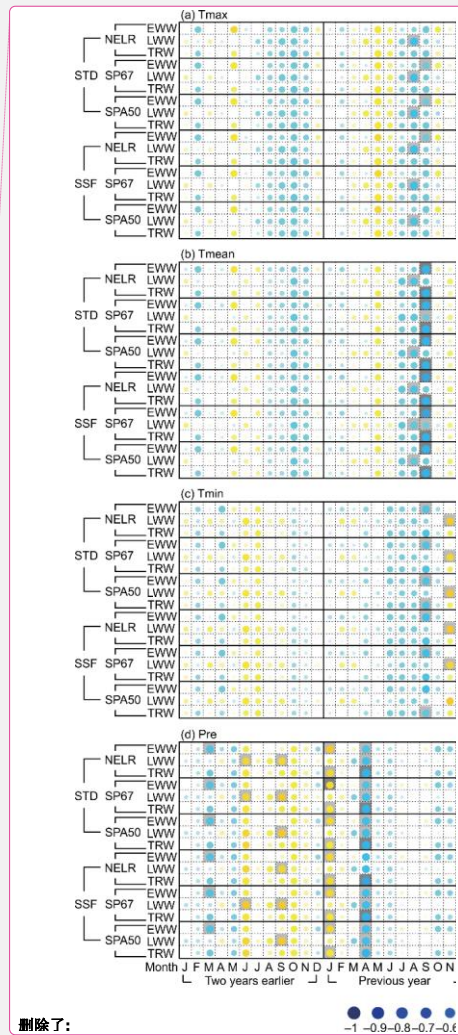


Figure 4. Matrix plots for the correlation coefficients between the prewhitened and linearly detrended tree-ring width chronologies and monthly climate time series from January of two years earlier to October of the current year. The climatic



删除了:

删除了: Correlation coefficients between the prewhitened and linearly detrended tree-ring width chronologies and climate time series. The explanations and legends are the same as Figure 3.

factors are monthly **(a)** maximum temperature (Tmax), **(b)** mean temperature (Tmean), **(c)** minimum temperature (Tmin), **(d)** total precipitation (Pre), **(e)** SPEI of 1-month scale, **(f)** SPEI of 3-month scale, **(g)** SPEI of 12-month scale, and **(h)** scPDSI. EWW, LWW, and TRW represent the earlywood width, latewood width, and total tree-ring width, respectively. The correlation analyses were conducted for the period 1953–2005 for the scPDSI, and for 1957–2005 for the other climatic factors. NELR, SP67, and SPA50 indicate the three detrending methods: (1) negative exponential functions combined with linear regression with negative (or zero) slope (NELR), (2) cubic smoothing splines with a 50 % frequency cutoff of 67 % of the series length (SP67), and (3) age-dependent splines with an initial stiffness of 50 years (SPA50). STD and SSF indicate the two standardization methods “standard” and “signal-free”, respectively. The correlation coefficients are reflected by the colorful and different-size circles, which can be referred to the color bar as shown at the bottom of the figure. The squares filled with light and dark gray color indicate that the correlation coefficients are statistically significant at the 0.05 and 0.01 level, which are tested using the Monte Carlo method (Efron and Tibshirani, 1986; Macias-Fauria et al., 2012).

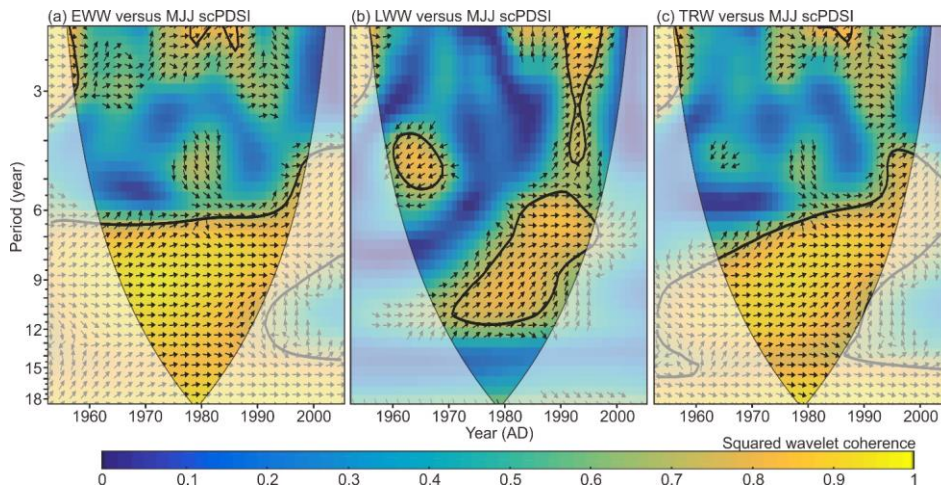


Figure 5. Squared wavelet coherence and phase relationship between the NELR based tree ring-width STD chronologies and MJJ scPDSI. (a–c) represent the results for EWW, LWW, and TRW, respectively. The color bar indicates the squared wavelet coherence. The arrows indicate the phase relationship with in-phase (anti-phase) pointing right (left), and MJJ scPDSI leading (lagging) tree-ring width with 90° pointing straight up (down). The thick contour indicates the 5% significance level against red noise. The cone of influence (COI) where edge effects might distort the picture is marked in a lighter shade.

删除了: shown as

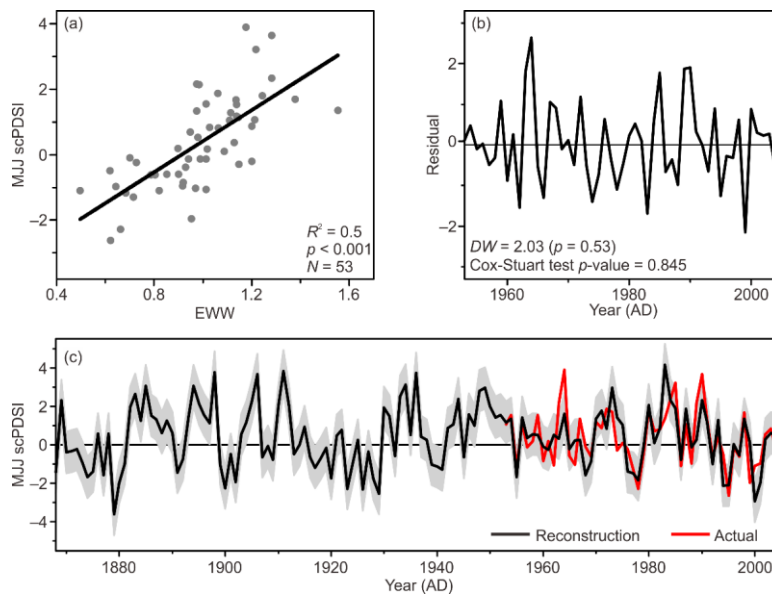


Figure 6. MJJ scPDSI reconstruction using NELR based EWW STD chronology. (a) Scatter diagram for the period 1953–2005, and (b) the resulting residuals. (c) MJJ scPDSI reconstruction (black line, after variance adjusted) and instrumental MJJ scPDSI (red line). Shaded area denotes the uncertainties of reconstruction in the form of ± 1 root mean square error.

删除了: during

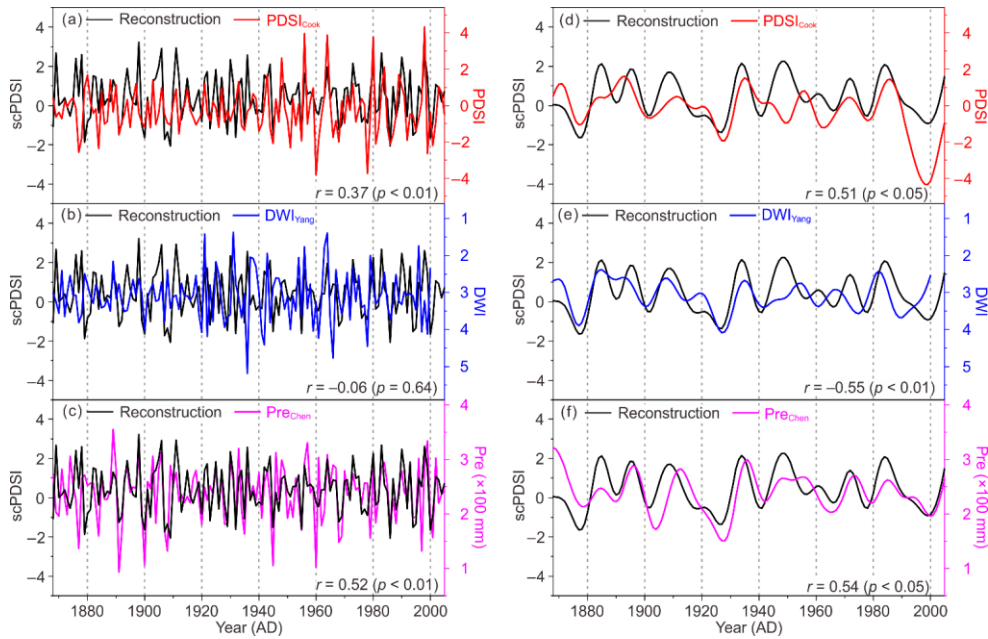


Figure 7. Comparison of the reconstructed MJJ scPDSI (black line) with other hydroclimatic reconstructions in adjacent regions on the interannual (left panels), and decadal and longer timescales (right panels). The referenced reconstructions are

5 (a, d) June–August PDSI of MADA NO. 370 point (Cook et al., 2010), (b, e) reversed DWI (Yang et al., 2013), and (c, f) TRW based April–June precipitation (Pre) reconstruction (Chen et al., 2016b). The interannual and decadal and longer fluctuations were separated using the adaptive 10 point “Butterworth” low-pass filter with 0.1 cutoff frequency (Mann, 2008). r represents the Pearson correlation coefficient between the reconstructed MJJ scPDSI and other hydroclimatic reconstruction over their common period. The significance level for all correlation coefficients were tested using the Monte Carlo method

10 (Efron and Tibshirani, 1986; Macias-Fauria et al., 2012).

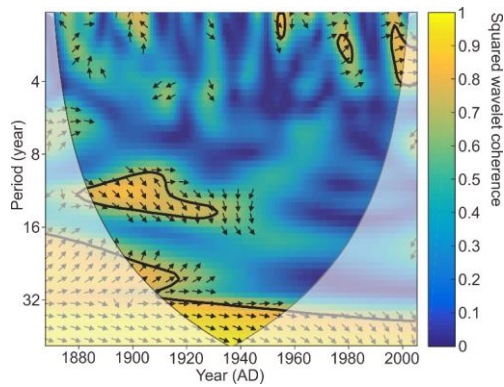


Figure 8. Squared wavelet coherence and phase relationship between the reconstructed MJJ scPDSI and EASMI (Zhao et al., 2015). The color bar indicates the squared wavelet coherence. The arrows indicate the phase relationship with in-phase (anti-phase) pointing right (left), and EASM leading (lagging) scPDSI with 90° pointing straight up (down). The thick contour indicates the 5 % significance level against red noise. The cone of influence (COI) where edge effects might distort the picture is marked in lighter shade.

删除了: shown as a

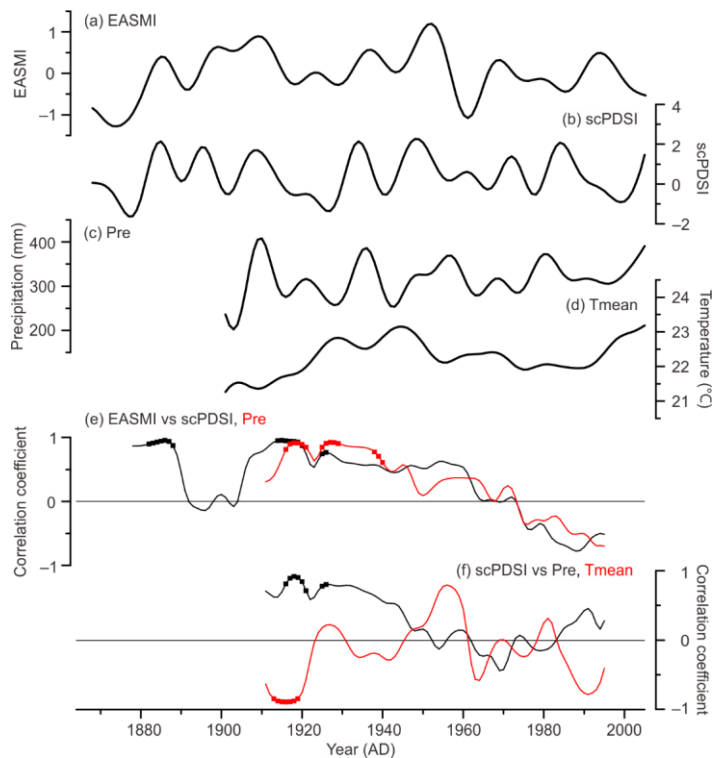


Figure 9. Comparison between the decadal and longer fluctuations of May–July (a) EASMI (Zhao et al., 2015), (b) reconstructed scPDSI, (c) precipitation (Pre; GPCC v7; Schneider et al., 2015), and (d) mean temperature (Tmean; CRU TS 4.01; Harris et al., 2014) over the area of reconstruction, (e) 21-year moving Pearson correlation coefficients of the decadal-filtered EASMI with scPDSI (black), and Pre (red). (f) 21-year moving Pearson correlations of the decadal filtered scPDSI with Pre (black), and Tmean (red). The decadal and longer fluctuations were derived using the adaptive 10 point “Butterworth” low-pass filter with 0.1 cutoff frequency (Mann, 2008). Statistically significant ($p < 0.05$) correlations are denoted as squares, which were tested using the Monte Carlo method (Efron and Tibshirani, 1986; Macias-Fauria et al., 2012).

删除了: 2017

删除了: ed area

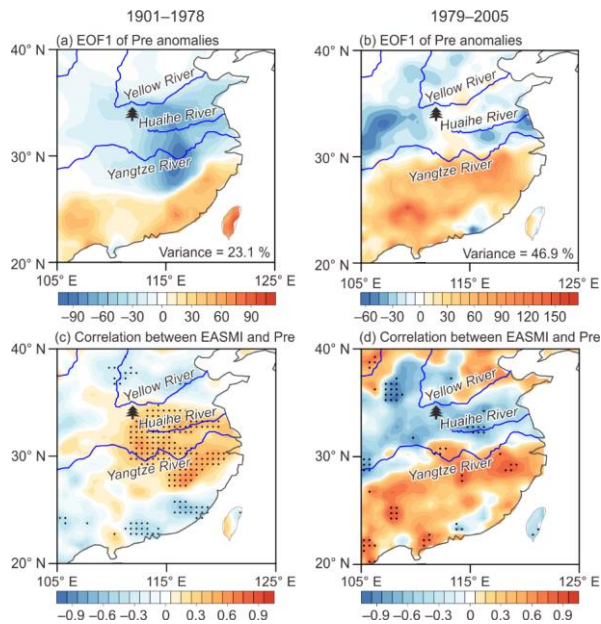


Figure 10. (a–b) The leading empirical orthogonal function (EOF) modes of decadal filtered May–July GPCP Precipitation anomalies for the periods 1901–1978 (left panel) and 1979–2005 (right panel). The color bar indicates the EOF values. **(c–d)** Spatial correlations between the decadal filtered May–July EASMI defined by Zhao et al. (2015) and precipitation (Pre) for the periods 1901–1978 (left panel) and 1979–2005 (right panel). The color bar indicates the correlation coefficient. Dots indicate correlation significant at $p < 0.1$. Decadal-scale and long-term fluctuations of precipitation were derived using the adaptive 10 point “Butterworth” low-pass filter with 0.1 cutoff frequency (Mann, 2008). The tree symbol denotes the study region.

删除了: indicated

删除了: P

删除了: .

删除了: The

删除了: s

删除了: that the

删除了: is statistically

删除了: (

删除了:

删除了:)

删除了: which was tested using the Monte Carlo method (Efron and Tibshirani, 1986; Macias-Fauria et al., 2012).

删除了: The d

删除了: er

Supplementary material

Table S1. Correlation coefficients between the tree-ring width chronologies from the two study sites, Baiyunshan and Longchiman, over their common period 1850–2005.

Chronologies	Detrending method		
	NELR	SP67	SPA50
EWV STD	0.63 / 0.59	0.64 / 0.60	0.62 / 0.57
LWV STD	0.40 / 0.51	0.46 / 0.49	0.46 / 0.47
TRV STD	0.58 / 0.58	0.60 / 0.62	0.61 / 0.63
EWV SSF	0.64 / 0.60	0.57 / 0.53	0.55 / 0.49
LWV SSF	0.43 / 0.54	0.37 / 0.51	0.35 / 0.47
TRV SSF	0.57 / 0.57	0.50 / 0.54	0.50 / 0.54

Note: The correlation coefficients before (after) the slashes are for the original (prewhitened and linearly detrended) STD and SSF chronologies. All correlation coefficients are statistically significant at the 0.001 level based on Monte Carlo test (Efron and Tibshirani, 1986; Macias-Fauria et al., 2012).

Table S2. Descriptive statistics of the composite STD and SSF tree-ring width chronologies when EPS ≥ 0.85 .

Detrending method	Chronology	Starting year when EPS ≥ 0.85	Standard deviation	Mean sensitivity	First-order autocorrelation
NELR	EWV STD	1868	0.238	0.225	0.348
	LWW STD	1877	0.25	0.221	0.421
	TRW STD	1871	0.221	0.200	0.458
SP67	EWV STD	1871	0.235	0.222	0.354
	LWW STD	1877	0.247	0.227	0.38
	TRW STD	1871	0.218	0.200	0.439
SPA50	EWV STD	1867	0.234	0.223	0.328
	LWW STD	1875	0.245	0.225	0.384
	TRW STD	1866	0.215	0.200	0.42
NELR	EWV SSF	1868	0.245	0.226	0.382
	LWW SSF	1875	0.263	0.221	0.451
	TRW SSF	1868	0.227	0.200	0.479
SP67	EWV SSF	1868	0.245	0.225	0.397
	LWW SSF	1875	0.255	0.226	0.404
	TRW SSF	1871	0.227	0.201	0.48
SPA50	EWV SSF	1867	0.234	0.207	0.418
	LWW SSF	1875	0.246	0.214	0.426
	TRW SSF	1866	0.214	0.191	0.459

Note: All statistics were calculated using the R package “dplR” version 1.6.9 (Bunn et al., 2018).

Table S3. Statistics of the detrended ring-width series over their common period 1915–2005.

Detrending method	Chronology	Var _{pc1}	Rbar _{eff}	SNR	EPS
NELR	EWV STD	0.386	0.443	25.878	0.963
	LWW STD	0.328	0.358	18.175	0.948
	TRW STD	0.384	0.433	24.806	0.961
SP67	EWV STD	0.427	0.492	31.452	0.969
	LWW STD	0.353	0.400	21.702	0.956
	TRW STD	0.422	0.481	30.104	0.96
SPA50	EWV STD	0.411	0.471	29.007	0.967
	LWW STD	0.341	0.384	20.315	0.953
	TRW STD	0.404	0.459	27.607	0.965
NELR	EWV SSF	0.399	0.456	27.291	0.965
	LWW SSF	0.317	0.346	17.252	0.945
	TRW SSF	0.393	0.439	25.492	0.962
SP67	EWV SSF	0.453	0.520	35.298	0.972
	LWW SSF	0.366	0.417	23.308	0.959
	TRW SSF	0.441	0.504	33.033	0.971
SPA50	EWV SSF	0.474	0.539	37.994	0.974
	LWW SSF	0.352	0.399	21.627	0.956
	TRW SSF	0.431	0.491	31.354	0.969

Note: The common period for the tree–ring width dataset was calculated with the “common.interval” function in R package “dplr” version 1.6.9 (Bunn et al., 2018) based on a trade–off between the maximum number of series and years. The statistics, Var_{pc1}, Rbar_{eff}, SNR, and EPS represent the variance explained by the first eigenvector, effective chronology signal, signal–to–noise ratio, and expressed population signal, respectively. The Var_{pc1} was calculated using the Program ARSTAN40c (Cook and Krusic, 2006), and the other statistics were calculated using the R package “dplr” version 1.6.9 (Bunn et al., 2018).

Table S4. The meteorological stations utilized by CRU dataset (<http://www.cru.uea.ac.uk/data>) located in the area between latitudes 32° N and 34.5° N, and longitudes 111° E and 112° E.

Meteorological station	Longitude (°E)	Latitude (°N)	Climatic factor	Temporal cover
Lushi	111.03	34.05	Precipitation	1952.07–2013.12
			Temperature	1952.07–2016.12
Laohekou	111.73	32.43	Precipitation	1933.02–1933.11; 1934.01–1935.06; 1935.08–1935.12; 1936.08–1938.07; 1950.06–2005.06; 2005.08–2013.12
			Temperature	1951.01–2016.12
Yunxian	111.8	32.9	Precipitation	1933.03–1938.05; 1938.07–1947.10; 1950.03–1990.12; 1991.05; 1991.07–1991.08

Table S5. The reconstructed May–July (MJJ) scPDSI during the period 1868–2005.

Year	scPDSI	Year	scPDSI	Year	scPDSI	Year	scPDSI
1868	-1.427	1904	1.167	1940	-1.139	1976	-1.394
1869	2.307	1905	2.260	1941	-1.300	1977	-1.474
1870	-0.388	1906	3.654	1942	0.859	1978	-1.829
1871	-0.321	1907	-0.630	1943	1.046	1979	-0.046
1872	-0.227	1908	-0.080	1944	2.380	1980	2.065
1873	-0.918	1909	-0.777	1945	-0.656	1981	0.088
1874	-1.682	1910	2.045	1946	1.589	1982	0.859
1875	-1.374	1911	3.842	1947	0.986	1983	4.150
1876	0.564	1912	2.012	1948	2.809	1984	2.327
1877	-1.568	1913	-0.495	1949	2.950	1985	1.891
1878	0.570	1914	-0.006	1950	1.998	1986	-0.770
1879	-3.612	1915	0.939	1951	1.428	1987	1.851
1880	-1.984	1916	-0.636	1952	1.549	1988	-0.127
1881	-0.991	1917	-1.179	1953	1.160	1989	0.269
1882	1.958	1918	-0.710	1954	1.355	1990	2.320
1883	2.622	1919	-0.167	1955	-1.682	1991	1.194
1884	1.254	1920	-1.749	1956	1.415	1992	-0.991
1885	3.071	1921	0.497	1957	0.356	1993	1.288
1886	1.522	1922	0.758	1958	0.550	1994	-2.118
1887	1.321	1923	-2.279	1959	0.523	1995	-2.104
1888	0.624	1924	-1.072	1960	-0.107	1996	0.041
1889	1.254	1925	0.255	1961	-0.247	1997	-0.556
1890	0.624	1926	-2.325	1962	0.517	1998	1.341
1891	-1.441	1927	-0.341	1963	0.336	1999	0.115
1892	-0.743	1928	-1.782	1964	1.616	2000	-2.942
1893	1.462	1929	-2.527	1965	-0.241	2001	-1.963
1894	3.057	1930	1.931	1966	0.229	2002	0.289
1895	2.112	1931	1.495	1967	0.262	2003	0.624
1896	1.549	1932	-0.569	1968	-1.568	2004	0.517
1897	1.120	1933	2.514	1969	-0.878	2005	1.777
1898	3.768	1934	3.111	1970	1.355		
1899	-1.025	1935	0.523	1971	1.777		
1900	-2.238	1936	3.721	1972	0.839		
1901	-0.489	1937	0.423	1973	2.970		
1902	-1.923	1938	0.249	1974	1.428		
1903	0.544	1939	-1.018	1975	1.020		

带格式表格

带格式表格

设置了格式: 英语(英国)

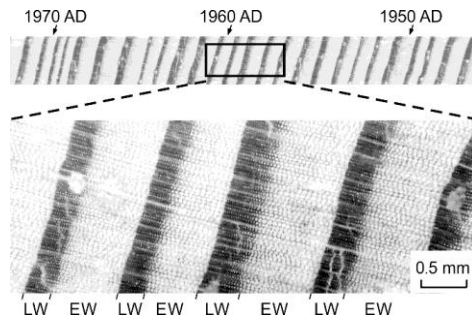


Figure S1. Photograph of a section of *P. tabulaeformis* tree-ring sample (LCM0118A). The distinct earlywood (EW) and latewood (LW) segments can be identified by inspection under a microscope.

删除了: Scanned p

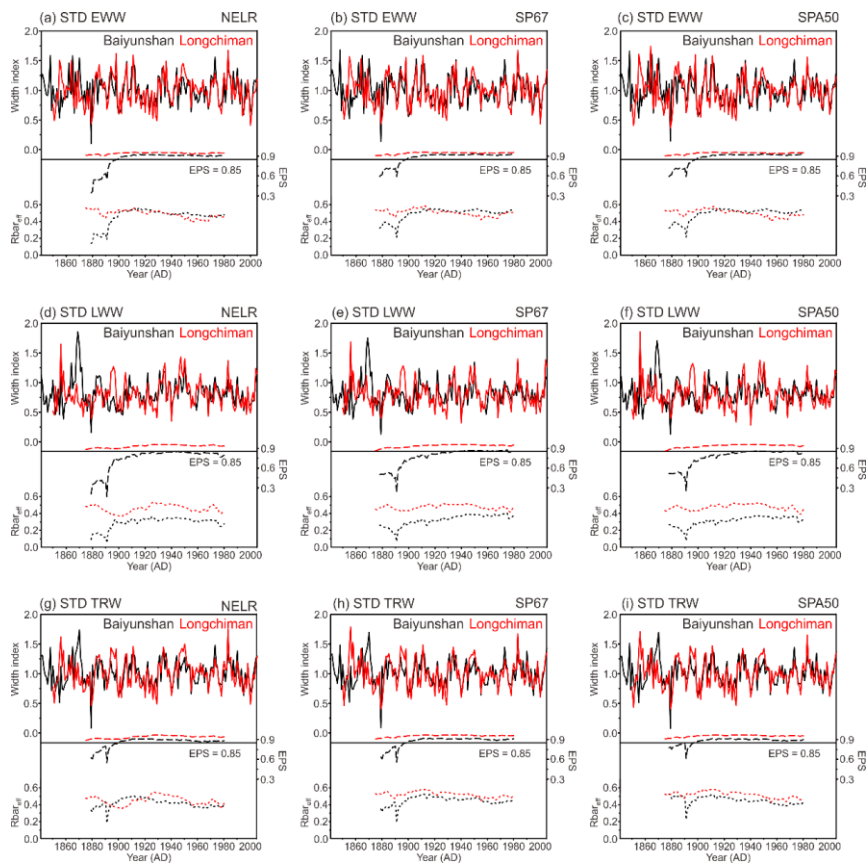


Figure S2. Standard (STD) tree-ring width chronologies (solid curves) generated using three kinds of detrending methods for (a–c) earlywood width (EWW), (d–f) latewood width (LWW), and (g–i) total tree-ring width (TRW) at the two study sites, Baiyunshan (black) and Longchiman (red). The three kinds of detrending methods are: (1) negative exponential functions combined with linear regression with negative (or zero) slope (NELR), (2) cubic smoothing splines with a 50 % frequency cutoff of 67 % of the series length (SP67), and (3) age-dependent splines with an initial stiffness of 50 years (SPA50). The dashed and dotted curves denote the running expressed population signal (EPS) and effective chronology signal ($Rbar_{eff}$), respectively. The horizontal line indicates the threshold EPS value of 0.85. The running EPS and $Rbar_{eff}$ values were calculated over a 51-year window.

删除了: together

删除了: ed

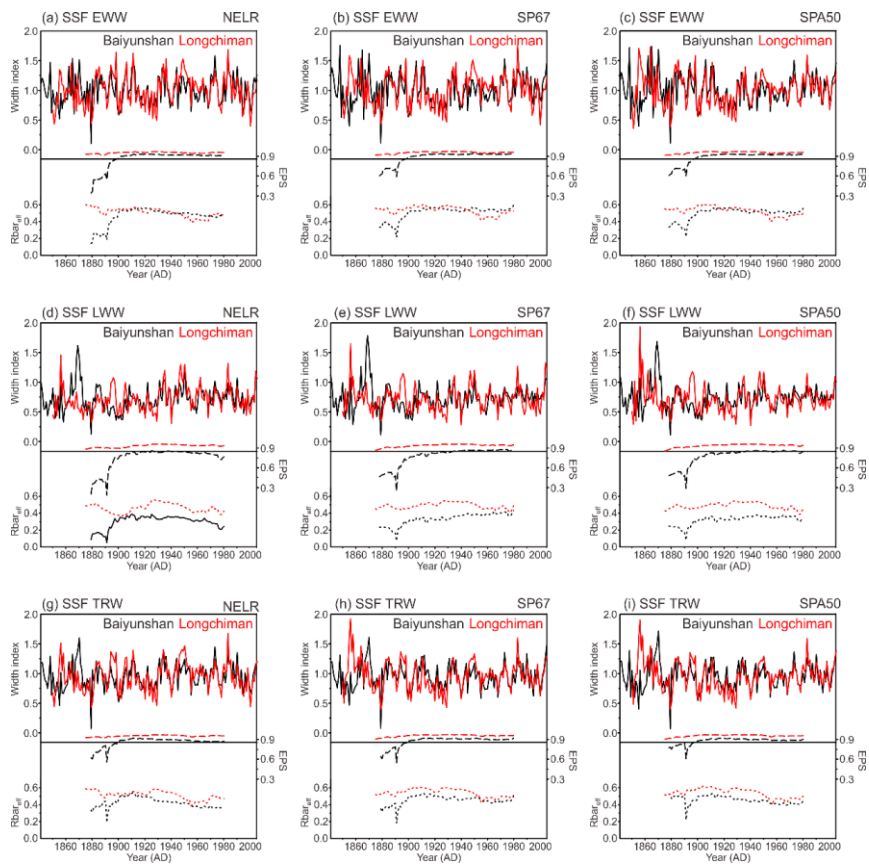


Figure S3. Signal-free (SSF) tree-ring width chronologies (solid curves) generated using three kinds of detrending methods for (a–c) earlywood width (EWW), (d–f) latewood width (LWW), and (g–i) total tree-ring width (TRW) at the two study sites, Baiyunshan (black) and Longchiman (red). The three kinds of detrending methods are: (1) negative exponential functions combined with linear regression with negative (or zero) slope (NELR), (2) cubic smoothing splines with a 50 % frequency cutoff of 67 % of the series length (SP67), and (3) age-dependent splines with an initial stiffness of 50 years (SPA50). The dashed and dotted curves denote the running expressed population signal (EPS) and effective chronology signal ($Rbar_{eff}$), respectively. The horizontal line indicates the threshold EPS value of 0.85. The running EPS and $Rbar_{eff}$ values were calculated over a 51-year window.

删除了: The same as Figure S2, but for the signal-free (SSF) chronologies. .

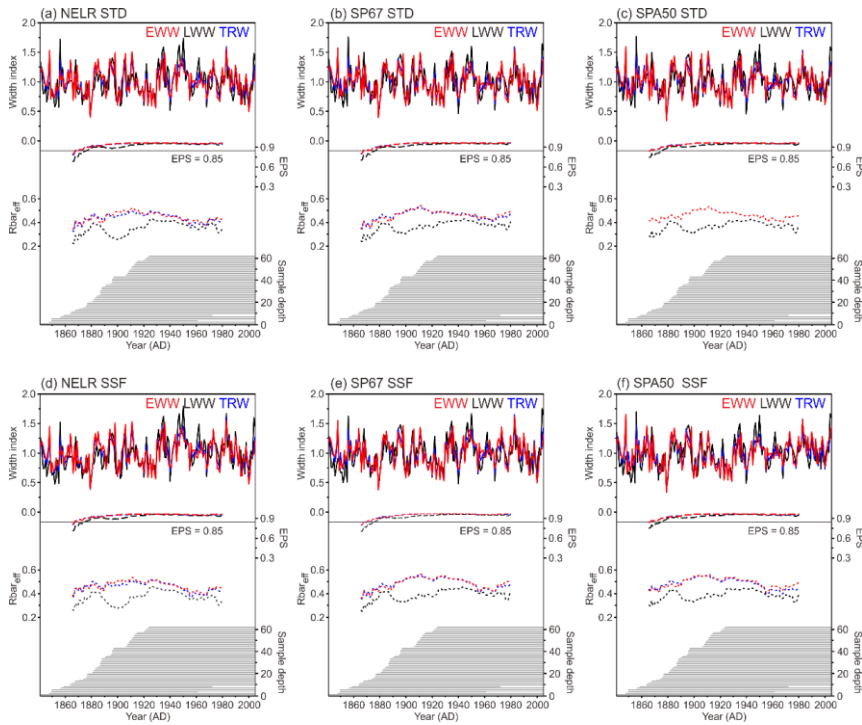


Figure S4. Composite (a–c) STD and (d–f) SSF tree-ring width chronologies for EWW (red), LWW (black), and TRW (blue) generated using the merged tree-ring samples from the two study sites, Baiyunshan and Longchiman, based on three kinds of detrending methods. The detrending methods are: (1) negative exponential functions combined with linear regression with negative (or zero) slope (NELR), (2) cubic smoothing splines with a 50 % frequency cutoff of 67 % of the series length (SP67), and (3) age-dependent splines with an initial stiffness of 50 years (SPA50). The dashed and dotted curves denote the running expressed population signal (EPS) and effective chronology signal ($Rbar_{eff}$), respectively. The horizontal line indicates the threshold EPS value of 0.85. The running EPS and $Rbar_{eff}$ values were calculated over a 51-year window. The segment plot indicated the sample depth (core).

删除了: together

删除了: ed

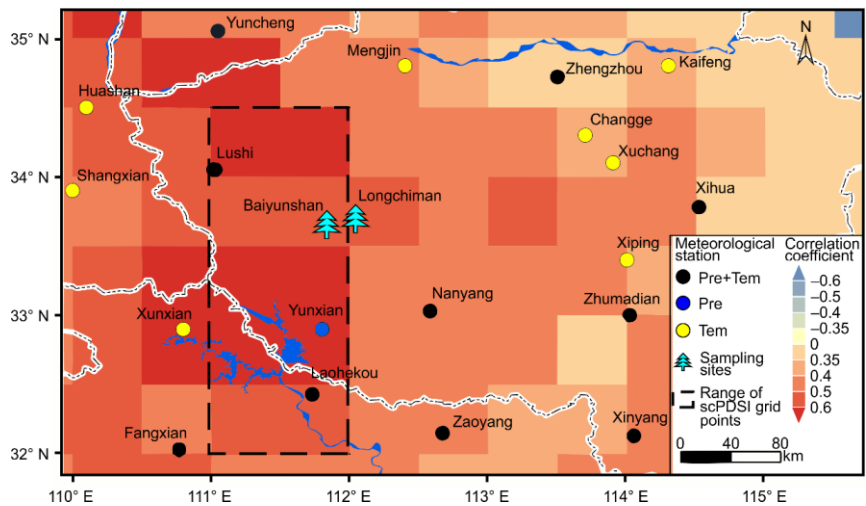


Figure S5. Spatial distribution of the meteorological stations included in the CRU dataset (<http://www.cru.uea.ac.uk/data>) around the tree-ring sampling sites, Baiyunshan and Longchiman. Black circles represent the meteorological stations that provide both precipitation and temperature data. While, Blue (yellow) circles represent those that only provide precipitation (temperature) data. The dashed rectangle indicates the range of scPDSI grid points used for calibration in this study. The color patches denote the spatial correlation coefficients between May-July scPDSI and NELR based EWW STD chronology.

删除了: blue

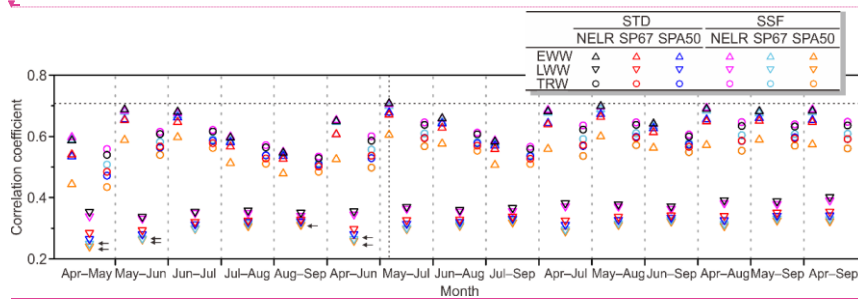
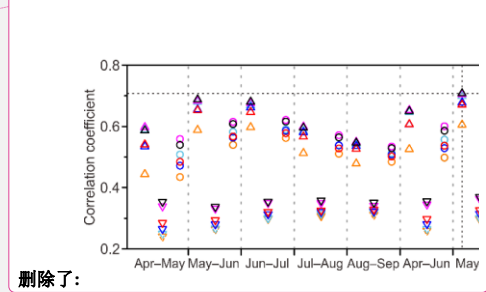


Figure S6. Correlation coefficients between the tree-ring width chronologies and multi-month averaged scPDSI (April to September of the current year). Upward triangles, downward triangles, and circles indicate the chronologies of EWW, LWW, and TRW, respectively. The color black, red and blue indicate the STD chronologies generated using the detrending methods NELR, SP67, and SPA50, while colors magenta, cyan, and orange indicate the SSF chronologies generated using the detrending methods NELR, SP67, and SPA50, respectively. The arrow indicates that the corresponding correlation does not reach the 0.05 significance level, which was tested using the Monte Carlo method (Efron and Tibshirani, 1986; Macias-Fauria et al., 2012).



删除了:

删除了: The u

删除了: respectively. The color

删除了: dashed symbol

删除了:

删除了: were

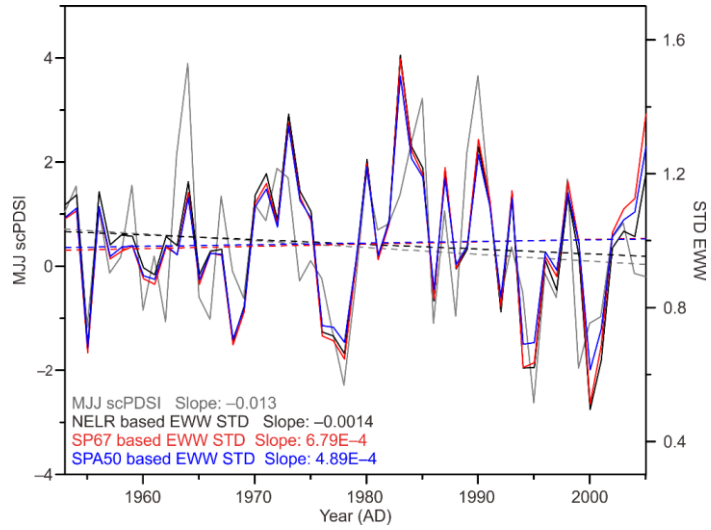


Figure S7. Comparisons between the MJJ scPDSI (gray) and EWW STD chronologies generated using the detrending methods NELR (black), SP67 (red), and SPA50 (blue) during the period 1953–2005. The corresponding linear trends are indicated by the dashed lines, and the slope statistics are labelled in the bottom left corner of the figure.

References

Bunn, A., Korpela, M., Biondi, F., Campelo, F., Mérian, P., Qeadan, F., Zang, C., Pucha-Cofrep, D., and Wernicke, J.: [dplR: Dendrochronology Program Library in R](https://CRAN.R-project.org/packages=dplR), <https://CRAN.R-project.org/packages=dplR>, r package version 1.6.9, 2018.

Cook E.R., Krusic P.J.: ARSTAN 41: a tree-ring standardization program based on detrending and autoregressive time series modeling, with interactive graphics, Tree-Ring Laboratory, Lamont Doherty Earth Observatory of Columbia University, New York, 2006.

Efron, B., and Tibshirani, R.: Bootstrap methods for standard errors, confidence intervals, and other measures of statistical accuracy, *Stat. Sci.*, 1, 54–77, 1986.

Macias-Fauria, M., Grinsted, A., Helama, S., and Holopainen, J.: Persistence matters: Estimation of the statistical significance of paleoclimatic reconstruction statistics from autocorrelated time series, *Dendrochronologia*, 30, 179–187, <https://doi.org/10.1016/j.dendro.2011.08.003>, 2012.